# Airborne validation of cirrus cloud properties derived from CALIPSO lidar measurements: Optical properties

Dennis L. Hlavka,[1,2] John E. Yorks,[1,2] Stuart A. Young,[3] Mark A. Vaughan,[4] Ralph E. Kuehn,[5] Matthew J. McGill,[6] and Sharon D. Rodier[1,4]

[1]   The Cloud-Aerosol Lidar Infrared Pathfinder Satellite Observations (CALIPSO) satellite was successfully launched in April 2006 to study cloud and aerosol layers using range-resolved laser remote sensing. Dedicated flights were conducted from July 26 to August 14, 2006 using the airborne Cloud Physics Lidar (CPL) to validate the CALIPSO lidar (CALIOP) data products. This paper presents results from coincident ice cloud measurements of lidar ratio, extinction coefficient, and optical depth. Flight segment case studies are shown as well as statistics for all coincident measurements during this CALIPSO-CloudSat Validation Experiment (CC-VEX). For the penetrated portion of opaque layers, CALIOP estimates of lidar ratio and extinction are substantially lower than the corresponding CPL values. Significant differences were also found for measurements of horizontally aligned ice, where different instrument viewing geometries precluded meaningful comparisons. After filtering the data set to exclude these discrepancies, overall CALIOP lidar ratio and extinction averages compared favorably to within 1% of overall CPL averages. When restricting the data further to exact coincident in-cloud point-pairs, CALIOP lidar ratios remained close to CPL values, averaging 2.1% below CPL, and the retrieved extinction and optical depth averaged 14.7% above CPL values, a result partially of higher average CALIOP attenuated backscatter but still a respectably close match.

## 1.   Introduction

[2]   Cirrus clouds have an important influence on the earth's climate system and radiation budget, which remains a significant uncertainty in understanding and predicting the climate system [*Stephens et al.*, 1990; *Intergovernmental Panel on Climate Change*, 2007]. A global climatology of ice cloud optical and spatial properties is necessary to improve estimates of cloud radiative processes in Global Climate Models. An important tool for improving the accuracy of cirrus optical and spatial property measurements is space-based atmospheric lidar. Space-based elastic back-scatter lidars such as the Geoscience Laser Altimeter System (GLAS) [*Spinhirne et al.*, 2005] and the Cloud-Aerosol Lidar with Orthogonal Polarization (CALIOP) [*Hunt et al.*, 2009] provide global statistics of optically thin cirrus cloud properties to the limit of signal attenuation with high temporal and spatial resolution that are not possible using in situ measurements [*Wang and Sassen*, 2001]. CALIOP, a dual wavelength, polarization-sensitive lidar, is the primary payload aboard the Cloud-Aerosol Lidar Infrared Pathfinder Satellite Observations (CALIPSO) satellite [*Winker et al.*, 2007]. The CALIOP level 1 and 2 standard data products report spatial and optical properties of both clouds and aerosols [*Winker et al.*, 2010]. CALIOP data has already been used extensively in global studies of cirrus spatial distributions [*Nazaryan et al.*, 2008; *Sassen et al.*, 2008] and the role of atmospheric dynamics in determining cirrus optical properties [*Martins et al.*, 2011]. CALIOP measurements and retrievals are also essential to regional studies that, for example, establish the role of the tropical eastern jet in the formation of cirrus layers during the Asian summer monsoon [*Das et al.*, 2011], investigate cloud formation mechanisms [*Riihimaki and McFarlane*, 2010] and ice nucleation processes [*Jensen et al.*, 2010] in the tropical tropopause, and provide guidance for improved model

[1]Science Systems and Applications, Inc., Lanham, Maryland, USA.
[2]NASA Goddard Space Flight Center, Greenbelt, Maryland, USA.
[3]CSIRO Marine and Atmospheric Research, Aspendale, Victoria, Australia.
[4]NASA Langley Research Center, Hampton, Virginia, USA.
[5]Cooperative Institute for Meteorological Satellite Studies, University of Wisconsin-Madison, Madison, Wisconsin, USA.
[6]Mesoscale Atmospheric Processes Laboratory, NASA Goddard Space Flight Center, Greenbelt, Maryland, USA.

Corresponding author: D. L. Hlavka, NASA Goddard Space Flight Center, Code 612, Bldg. 33, Room A415, Greenbelt, MD 20771, USA. (dennis.l.hlavka@nasa.gov)

parameterizations of Arctic mixed-phase clouds [*Gayet et al.*, 2009].

[3] Since CALIOP data is widely used for studying cirrus properties, it is necessary to assess the accuracy of the cirrus cloud measurements reported in the standard data products. However, to date few such studies exist. *Dupont et al.* [2009] used four ground based lidars to assess the spatial and optical properties of cirrus reported in the CALIPSO version 2 (V2) data products. *Mioche et al.* [2010] also used V2 data to compare co-located airborne lidar backscatter and in situ extinction measurements to CALIOP retrievals. Using CALIPSO version 3 (V3) data products, *Thorsen et al.* [2011] compared CALIOP cloud heights and optical depths to ground-based measurements acquired over a 31 month period in the tropical west Pacific.

[4] The Cloud Physics Lidar (CPL) [*McGill et al.*, 2002], an airborne, multiwavelength, polarization-sensitive elastic backscatter lidar, is arguably the most comprehensive cirrus cloud validation tool for CALIOP data products. Between July 26 and August 14 2006, CPL was a payload on the NASA ER-2 aircraft as part of validation flights during the CALIPSO and CloudSat Validation Experiment (CC-VEX) [*McCubbin et al.*, 2006]. The CALIOP level 1 calibrated backscatter profiles and level 2 layer detection were examined for specific cirrus cloud case studies using CPL data by *McGill et al.* [2007]. *Yorks et al.* [2011b] evaluated statistics of transparent cirrus cloud spatial properties reported in the CALIOP level 2 standard data products with CPL products. Overall, these studies establish good agreement between the spatial properties of cirrus clouds measured by both instruments, especially during nighttime hours when the signal-to-noise ratio (SNR) is higher for both instruments.

[5] Attenuated backscatter coefficients, feature detection, and boundary location are essential elements in accurately resolving optical properties such as extinction-to-backscatter ratio or lidar ratio ($S_p$) and extinction coefficient. Discrepancies above 15% in lidar ratio can lead to significant discrepancies in the resultant extinction, which further lead to significant radiative flux discrepancies. In this study, we compare the optical properties of ice clouds from the 5 km Version 3.01 Level 2 CALIOP products to collocated CPL measurements at identical spatial scales, determine the differences between the lidar ratio and extinction retrieved by the two instruments, and determine the frequency and origin of these differences.

## 2. Lidar Ratio and Extinction Algorithms

[6] Algorithms discussed in this section focus on CPL optical retrievals. Because these are similar to the CALIOP algorithms with noted exceptions and because CALIOP algorithms are well-documented in the literature, a separate section will not be devoted to the CALIOP algorithms. Refer to section 3.2 for CALIOP algorithm references and a detailed discussion of the algorithm differences between the two systems.

[7] The primary atmospheric observation channel of CPL and CALIOP for this study is 532 nm. Gas absorption processes, apart from ozone, are negligible compared to scattering processes at this wavelength. Ozone absorption, although small, is corrected for in the CPL analysis prior to

the optical properties algorithm by using ozone transmittance profiles derived from ozone climatological databases.

[8] When attempting to obtain cloud optical depth from a spacecraft or aircraft elastic backscatter lidar, two assumptions are required regarding the scattering characteristics of the cloud. One is that multiple scattering effects can be reliably quantified by a correction factor (discussed in section 3.1.3). The second is that the value of the particulate lidar ratio ($S_p$) is known. For a given scattering layer for CPL processing, $S_p$ is assumed to be constant. In cases of transparent cloud layers and no or very weak background aerosol loading this ratio can be estimated from the lidar data itself. Otherwise, solving the lidar equation will require assumed values retrieved from a look-up table or values based on an available quantity such as depolarization ratio or temperature. The values of both assumed parameters are determined by the details of the volumetric scattering phase function that quantifies light scattering as a function of scattering angle. The validity of the above assumptions relies strongly upon former experience with cirrus lidar observations [*Spinhirne and Hart*, 1990; *Spinhirne et al.*, 1996].

### 2.1. Transmittance Solution to the Lidar Equation

[9] CPL data products report particulate layer $S_p$, particulate extinction coefficient profiles ($\sigma_p(z)$) and particulate layer optical depths ($\tau_p$) for cloud and aerosol layers. These cloud and aerosol optical properties are derived as outlined below and demonstrated by *Spinhirne et al.* [1980, 1996], *Elouragini* [1995] and *Marenco et al.* [1997]. Transmittance, extinction, and optical depth estimates obtained directly from the solution of the lidar equation are actually the apparent, or effective, values [*Platt*, 1979] which include multiple-scattered photons.

[10] The lidar equation for a high-altitude nadir-pointing lidar with photon counting detectors can be rewritten in the following form:

$$\beta'(r) = \beta(r)T^2(r) = \frac{(n(r)D(n) - n_b)r^2}{O(r)ECT^2_{O_3}(r)}. \quad (1)$$

The raw lidar signal is represented by $n(r)$ as a function of range (r) from the lidar. $D$ represents the dead time correction as a function of signal strength needed when using photon counting detectors. The solar background signal is $n_b$. Other instrument corrections are the near field overlap correction ($O$) and outgoing energy normalization factor ($E$). The system calibration is $C$ and the ozone transmittance factor is $T^2_{O_3}$. The left side of the equation is the attenuated backscatter coefficient corrected for ozone attenuation. The parameter is the product of the total (particulate and molecular) volumetric backscatter coefficient at range $r$ denoted by $\beta(r)$ and the two-way total effective transmittance factor is expressed as $T^2(r)$. This transmittance is equivalent to $\exp[-2(\tau_m(r) + \eta\tau_p(r))]$, where optical depth is represented by the symbol $\tau$, and the subscripts $m$ and $p$ designate molecular and particulate contributions, respectively. The influence of the multiple scattering factor ($\eta$) on the particulate optical depth between an initial range $r_0$ and r is described by:

$$\eta\tau_p(r) = \int_{r_0}^{r} \eta(r)\sigma_p(r)dr \cong \bar{\eta}\int_{r_0}^{r}\sigma_p(r)dr, \quad (2)$$

where $\sigma_p$ is particulate extinction. CPL multiple scattering effects are for the most part close to negligible [*McGill et al.*, 2003] as discussed in section 3.1.3, and thus for all CPL data analysis, $\eta$ is set to unity.

[11] Since the molecular contribution to the total backscatter and transmittance can be computed from theory, it is essential to separate the scattering terms into components which represent the molecular and particulate contributions independently.

[12] The attenuated backscatter expansion becomes:

$$\beta' = \beta_p T_p^{2\eta} T_m^2 + \beta_m T_p^{2\eta} T_m^2. \qquad (3)$$

The following relationships must now be defined:

$$T_p^{2\eta}(r) = \exp\left(-2\eta \int_{r_0}^{r} \sigma_p(r)dr\right) \quad \text{and} \quad \eta S_p = \frac{\eta \sigma_p}{\beta_p} \qquad (4)$$

and

$$T_m^2(r) = \exp\left(-2 \int_{r_0}^{r} \sigma_m(r)dr\right) \quad \text{and} \quad S_m = \frac{\sigma_m}{\beta_m}, \qquad (5)$$

where $S_m$ and $\eta S_p$ are the molecular and effective particulate lidar ratios, respectively, and $\eta S_p$ is assumed to be a constant for each layer. $T_m^2(r)$ and $\beta_m(r)$ can be calculated accurately given the vertical temperature and pressure structure of the atmosphere from atmospheric profiles obtained using the World Meteorological Organization (WMO) Upper Air station radiosonde closest in space and in time to the ER-2 aircraft flight track and the fact that $S_m$ is known to be $8\pi/3$ throughout the vertical profile. Once the molecular backscatter coefficient and two-way molecular transmittance are computed, the lidar equation can be used to solve for the vertical profile of $T_p^2$ by the method outlined in the appendix of *Spinhirne et al.* [1980]. The actual particulate backscatter, optical depth, and extinction profiles can then be computed from the values of $S_p$, $T_p^2$, and $\eta$ using the relationships in equations (3), (4), and (5).

## 2.2. Determination of Lidar Ratio

[13] An essential ingredient in deriving particulate transmittance profiles is the effective lidar ratio ($\eta S_p$). We consider here four basic categories for determining lidar ratios: constrained, unconstrained default, modified default, and opaque. A discussion of each follows.

[14] When a layer being analyzed is transparent (with either a lower layer or the earth's surface sensed) and resides within otherwise pristine air (no aerosols) so that it is possible to determine transmittance loss through the layer, then an algorithm to calculate an estimate of $\eta S_p$ is called. If $\eta S_p$ is found to be within tolerances, currently between 8 and 100 sr, it will be used. Extinction solutions using lidar ratios calculated in this manner are categorized as "constrained." The algorithm first calculates an estimate of $T_p^{2\eta}(z_b)$, where $z$ is the vertical range and $z_b$ is to the bottom of the layer, then $\eta S_p$ can be found using an iterative process. The constrained algorithm is discussed in detail in section 2 of *Yorks et al.* [2011a]. This algorithm has been used for over ten years of CPL optical products and the constrained lidar

ratios derived from this procedure agree favorably with previous studies of lidar ratio [*Yorks et al.*, 2011a].

[15] For cloud layers where $\eta S_p$ cannot be calculated as described above due to high aerosol loading or low SNR or proximity to the earth's surface, a value will be assigned for each layer based on pre-defined relationships with layer integrated depolarization ratio retrieved from the 1064 nm channels of CPL or layer mean temperature from the radiosonde profile, with the depolarization ratio used if available. These relationships are based on the results presented by *Yorks et al.* [2011a]. Ice clouds, the focus of this study, have default lidar ratio values mostly in a tight range between 24 and 26 sr. If this lidar ratio remains unmodified through the solution process, we describe this category as "unconstrained default" or just default.

[16] During CPL processing with the default lidar ratio, if the $T_p^{2\eta}(z)$ term goes below the set limits before reaching the bottom of the cloud layer, an iterative process is invoked where the effective lidar ratio is reduced by 0.5 sr and the layer is reprocessed. This iterative reprocessing continues until the analysis can reach the bottom of the layer or the number of iterations reaches 30. We describe this condition as the "modified default" category.

[17] In CPL data processing, opaque layers are treated as special cases of the "constrained" lidar ratio algorithm. For the case of an opaque layer (defined in practical terms as a layer that has no layer sensed below it and no ground signal), the two-way particulate transmittance term at the "lidar" cloud bottom, where the lidar signal is extinguished, is set to an assumed value consistent with the lidar equation transmittance results just before the point of opaqueness (where the lidar equation becomes unstable). Currently, this value of $T_p^{2\eta}(z_b)$ is set to 0.004. The constrained lidar ratio is then calculated using this special $T_p^{2\eta}(z_b)$ value for input into the constrained lidar ratio algorithm. If the calculated lidar ratio value falls within thresholds, it is used; otherwise a default value is sent to start the full optical processing of the layer. The "opaque" lidar ratio and the resulting transmittance and extinction profiles only apply to the segment of the actual cloud above the height where the lidar signal is extinguished.

## 3. Validation Issues for Space-Based Lidar Extinction Retrievals

[18] Validation of extinction profiles retrieved from measurements by satellite-borne lidars like CALIOP is not an easy or straightforward task. The great distance of the lidar from the atmospheric target and the combination of a relatively low laser pulse rate, high speed across the target and high background light levels cause the SNR to be much lower than for airborne or ground-based lidars. Therefore, considerable averaging of the space-borne lidar signals is necessary before analysis and, because of spatial and temporal variability of the atmospheric targets, this can cause difficulties in comparing space-borne and other lidar data. There are also instrumental differences and different viewing geometries that can cause differences in the measured signals. This is particularly the case for clouds, which tend to be more variable and inhomogeneous than aerosols layers. Therefore, data sets for comparison and validation must be chosen carefully.
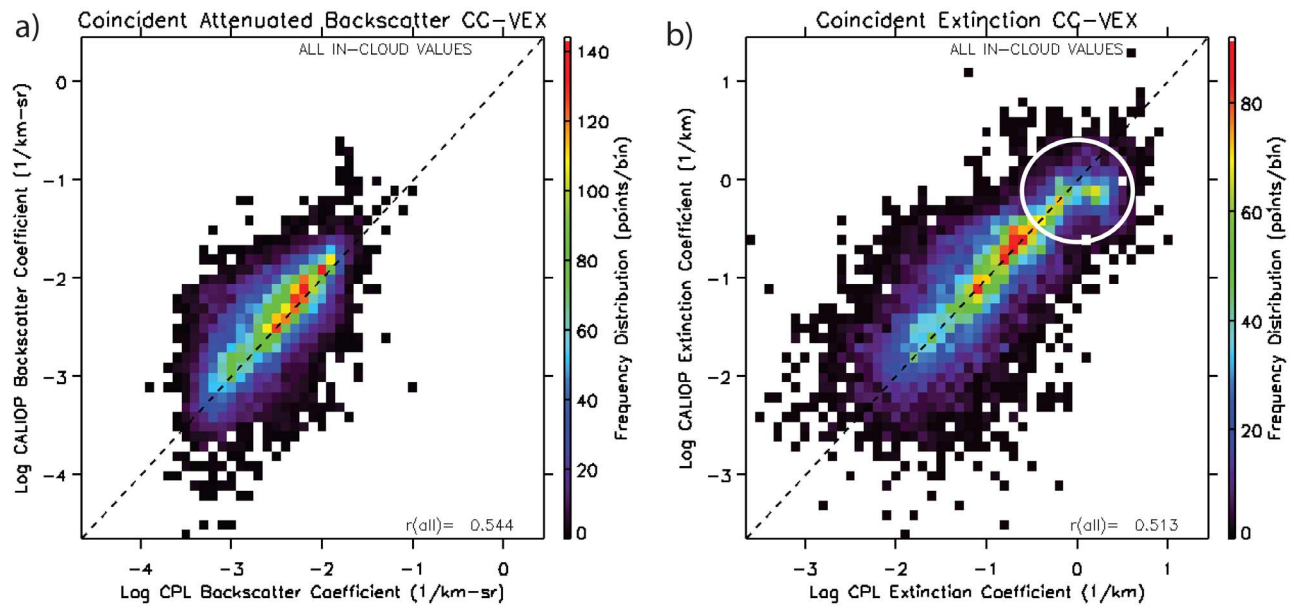
**Figure 1.** (a) Comparison of attenuated backscatter signals of coincident CC-VEX CALIOP-CPL point pairs using colors to denote bin frequencies. (b) Corresponding point pairs of the resulting extinction retrievals. The dashed lines represent the one-to-one correspondence fit. A CALIOP positive bias is evident in Figure 1a. The uncertainty in attenuated backscatter has a large impact on the uncertainty of the retrieved extinction coefficients. A difference in the extinction comparison in Figure 1b not related to backscatter is circled. Here differences in instrument algorithms during opaque cloud conditions are the main driver. To observe the comparison with the opaque conditions removed, see Figure 14a. Point pairs in both plots are restricted to data from randomly oriented ice crystals.

[19] CPL is a well-tested system with validated data products [*Schmid et al.*, 2003]. With its superior SNR that results from shorter distance to the target, lower transit velocity and hence greater number of profiles to average, CPL is more likely to detect tenuous cloud where it is present, to make accurate estimates of effective cloud transmittance and optical depth, and hence provide better constrained extinction retrievals. In short, the CPL is currently the best available instrument for validating CALIPSO extinction retrievals of cirrus under the elastic backscatter lidar assumptions.

[20] Although the data sets for comparison are chosen to be as spatially and temporally coincident as is feasible, there are still factors that can cause differences in the retrieved extinction profiles from the two instruments. These factors fall into two main classes; these are differences in the input signals and differences in the retrieval algorithms.

### 3.1. Differences in the Input Attenuated Backscatter Profiles

[21] There are two fundamental factors that will always ensure that the signal profiles from a space-borne lidar and an airborne lidar are different, even if the viewing geometries, system parameters and sampled atmospheric volume are the same. The first of these factors is calibration. As there is always some uncertainty in the calibration of any lidar, we should expect that there will be a difference between spacecraft and aircraft systems. Calibration errors are systematic errors and can cause biases between the retrievals from the different instruments. The second factor is random photon noise associated with both the detected signal and the

background. Differences in the signals due to random noise will be most obvious where the signals are weaker, such as in the lower regions of clouds where the signal has been significantly attenuated.

[22] These two effects are illustrated in Figure 1a where CALIOP attenuated backscatter signals are compared with coincident data from the CPL during CC-VEX using a probability density function (PDF) plot with the bin frequency color-coded. The figure contains 9511 point pairs comprising all coincident data during randomly oriented ice (ROI) conditions (see description in section 3.1.4). Here we take coincidence as meaning that the CALIOP-CPL point pairs had maximum spatial and temporal separations of 1716 m and 10 min respectively. The figure, which displays the frequency distribution of the point pair backscatter, indicates that most of the points lie on or near the dashed line, which represents one-to-one correspondence. The linear fit of the data is represented by the equation:

$$CALIOP = (0.992 \pm 0.0157) * CPL + (0.00183 \pm 0.000113)$$
$$\text{with } r = 0.544. \tag{6}$$

Overall, we can see that there is some bias in the CALIOP attenuated backscatter compared with CPL when all the data are considered, with CALIOP data averaging 10–20% higher than CPL when the backscatter strength is between 5.0e-03 and 2.0e-02 km$^{-1}$ sr$^{-1}$. Differences are seen for various subsets as shown in Table 1. We can see that there are some points where differences between CALIOP and CPL are large, as indicated by the large distances from the

**Table 1.** Linear Fit for Ice Cloud Attenuated Backscatter Coincidence (CALIOP = a*CPL+b) Excluding HOI

| Ice Cloud Category (Both Instruments) | Number of Points | a | a Uncertainty | b | b Uncertainty | Correlation Coefficient |
|---|---|---|---|---|---|---|
| All Bins | 9511 | 0.99190 | 0.01569 | 0.00183 | 0.00011 | 0.544 |
| All Bins Transparent | 7354 | 0.95449 | 0.01281 | 0.00114 | 0.00007 | 0.656 |
| Day Transparent | 2715 | 1.12874 | 0.02842 | 0.00083 | 0.00015 | 0.666 |
| Night Transparent | 4639 | 0.77627 | 0.01260 | 0.00163 | 0.00007 | 0.671 |
| Constrained Lidar Ratios | 1235 | 0.93716 | 0.02583 | 0.00182 | 0.00017 | 0.719 |
| Default Lidar Ratios | 3272 | 0.98991 | 0.01552 | 0.00075 | 0.00009 | 0.745 |
| Opaque Layers | 1618 | 0.58645 | 0.02438 | 0.00685 | 0.00024 | 0.513 |

dashed line. The differences can approach one and a half orders of magnitude. These differences result from different random noise in the signals and from other factors discussed below. This will lead directly to differences in the retrieved extinction profiles (Figure 1b), but such large differences are relatively infrequent. One difference in the extinction comparison in Figure 1b not related to the backscatter comparison is circled. Here differences in instrument algorithms during opaque cloud conditions are the main driver (see section 3.2.4).

### 3.1.1. Temporal and Spatial Sampling Differences

[23] During CC-VEX, great care was taken to fly the CPL as closely as possible to CALIPSO's ground track. For the experiment data set, the cross-track mismatch between the aircraft and satellite ground tracks varied between a minimum of 37 m and a maximum of 1716 m with an average of 835 m. However, CALIPSO travels at 7.5 km/s, whereas the CPL travels at ~0.2 km/s, so a collocated segment located ±10 CPL minutes from nearest coincidence will be covered by CALIPSO in only 35 s. During this period, processes such as cloud vertical motion and development and cloud advection due to winds varying with height will cause the atmosphere sampled by the two instruments to be different. Even at the temporal and spatial coincidence displayed in Figure 2a, differences can be seen in the attenuated backscatter profiles measured by CALIOP and the CPL, with resultant minor differences in the retrieved extinction profiles. These attenuated backscatter differences result from random noise (see above and below the main cloud layer) slight spatial offset (288 m) and the fact that the CALIOP footprint of ~90 m samples a much larger atmospheric volume than does the CPL footprint, which is only 1 m at the cloud top.

[24] As another example, Figure 2b illustrates profiles separated by only ~100 s. The attenuated backscatter profile structure is different and the more rapid decrease of the CPL signal with cloud penetration is apparent. Also note that the lower layer at ~11 km is proportionately smaller for the CPL signals than for CALIOP signals. The signal from the lower layer has, in fact, been reduced in magnitude to below the threshold of the CPL layer detection algorithm, with the result that the CPL analysis retrieves no extinction in this layer. Figure 2c displays the profile match when the instruments were offset by 247 s allowing for a wind drift of 4 km.
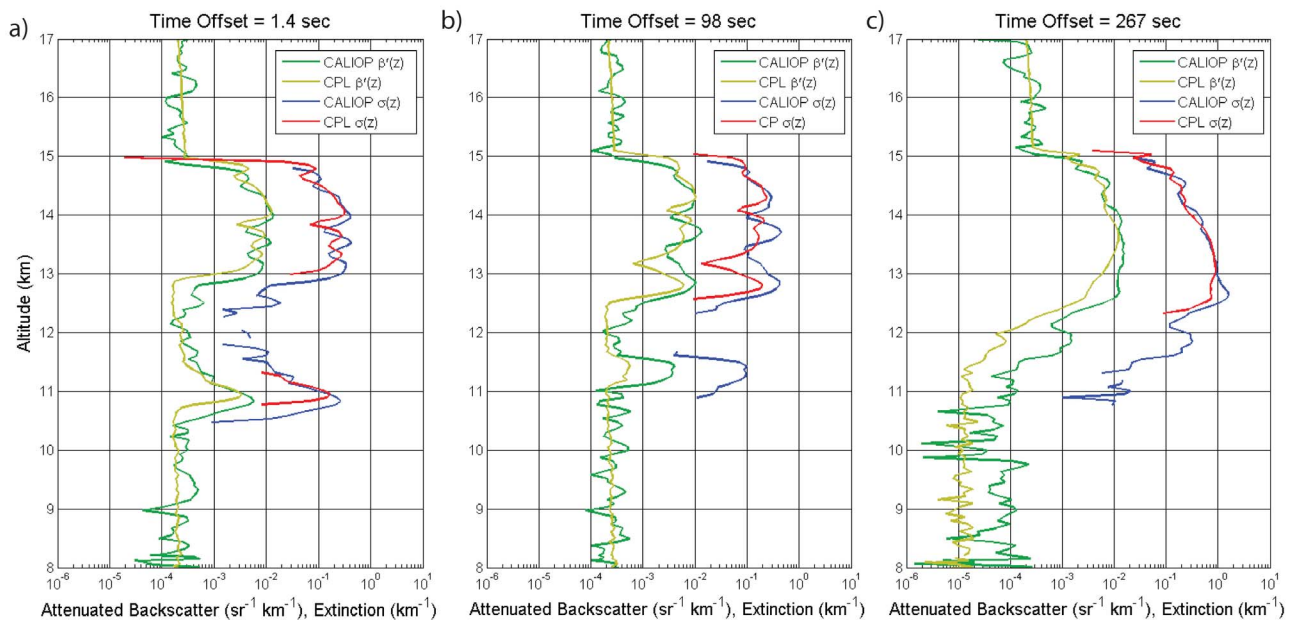


**Figure 2.** Attenuated backscatter profiles measured by CALIOP (green) and CPL (yellow) and extinction coefficient profiles estimated by CALIOP (blue) and CPL (red) during CC-VEX on 11 August 2006 (a) at the closest temporal and spatial coincidence (1.4 s) when separation was 288 m, (b) at a temporal offset of 98 s when separation was 340 m, and (c) at a temporal offset of 267 s when separation was 987 m and estimated wind drift was 4 km. Profiles are averaged 5 km horizontally.
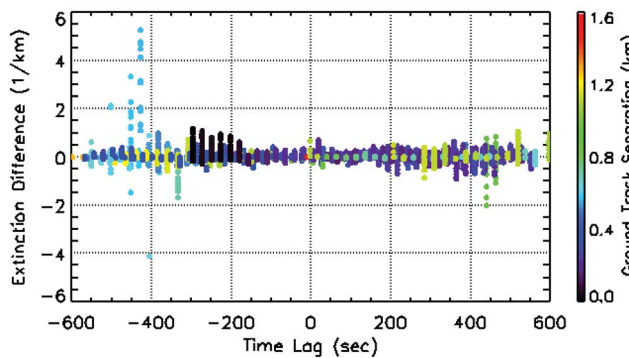
**Figure 3.** The effects of the spatial and temporal disparities (CALIOP-CPL) on extinction retrievals during CC-VEX are shown. The plot shows the effects the time difference (*x* axis) as well as the ground track offset (color code) have on the difference (CALIOP-CPL) in extinction between the two instruments (*y* axis). This plot was made using all transparent randomly oriented ice clouds in all the coincident segments

The effects of the spatial and temporal disparities are summarized in Figure 3. This plot shows the effects the time difference (*x* axis) as well as the ground track offset (color code) have on the difference (CALIOP-CPL) in extinction between the two instruments (*y* axis). In general, the time difference is more important than the track offset but the extinction difference is still acceptable even at 10 min time difference. This plot was made using all transparent ice ROI clouds in the coincident segments of CC-VEX.

### 3.1.2. Differences in SNR and Effects on Layer Detection

[25] Extinction retrievals from both CALIOP and CPL algorithms are restricted to only those portions of a profile where layers were detected. The collocated extinction comparisons shown in this work are thus from regions where the layer detection algorithms used by CALIOP and CPL both independently detected cirrus clouds. However, as explained by *Yorks et al.* [2011b], the considerable differences in SNR between CALIOP and CPL yield considerable differences in layer detection efficiency for results obtained at identical spatial resolutions. To overcome the SNR limitations imposed on space-based platforms, the CALIOP layer detection scheme searches for clouds and aerosols using a sequence of successively coarser spatial resolutions designed to detect successively weaker/fainter layers [*Vaughan et al.*, 2009]. Subsequent extinction retrievals are conducted only for those layers detected at 5 km, 20 km, and 80 km [*Young and Vaughan*, 2009]. The CALIPSO data products report cirrus cloud extinction coefficients at a uniform spatial resolution of 5 km horizontally and 60 m vertically, with the values for layers detected at the coarser spatial resolutions (i.e., 20 km and 80 km) being replicated as required at 5 km intervals along the full horizontal extent of the layer. The CPL data, on the other hand, has considerably better SNR than CALIOP data, and thus the CPL analysis can generate results using a single, fixed spatial resolution for both layer detection and extinction retrievals. The standard CPL data products are reported at a horizontal resolution of 200 m and a vertical

resolution of 30 m; however, for this study the CPL data was averaged to 5 km horizontally and 60 m vertically, in order to match the fundamental CALIOP detection resolution.

[26] If the layer is not homogeneous, the relationship between the CALIOP and CPL extinction values may become skewed. This occurs because the noise characteristics of the 532 nm CALIPSO data at lower signal levels are not Gaussian [*Wu et al.*, 2011] and because the solution to the lidar equation is nonlinear.

### 3.1.3. Differences in Multiple Scattering Effects

[27] The magnitude of multiple scattering contributions to the lidar backscatter signal depends on the lidar viewing geometry (transmitter divergence, receiver field of view (FOV), and distance to the target) and the scattering phase function of the particulates being measured [*Bissonette*, 2005]. The combination of the receiver FOV and distance to target defines the projected footprint of the lidar receiver system, and it is the size of this footprint relative to the photon mean free path in the scattering medium that largely determines the amount of multiple scattering present in the lidar signal [*Eloranta*, 1998]. Given a constant mean free path, a larger lidar footprint will result in greater contributions from multiple scattering because of the increased probability of multiple, off-axis scattering events occurring within the receiver FOV. Differences in multiple scattering in the CPL and CALIOP signals can thus be anticipated based on footprint size alone. At an ER-2 cruising altitude of 20 km, the CPL FOV of 100 $\mu$rad [*McGill et al.*, 2002] produces a footprint diameter of ~1 m at a cloud top altitude of 10 km. When measuring the same cloud, CALIOP's slightly larger FOV (130 $\mu$rad) and much greater distance above cloud top (nominal orbit altitude of ~705 km) result in a substantially larger footprint of ~90 m at cloud top [*Hunt et al.*, 2009].

[28] Both CPL and CALIOP analysts have employed simulations to characterize the effects of multiple scattering. Using the multiple scattering formalism developed by *Platt* [1973], *Winker* [2003] performed Monte Carlo calculations to compute $\eta$ values for the CALIPSO geometry for several different cirrus phase functions. The most significant finding of that work demonstrated that, for cirrus clouds, $\eta$ remains relatively constant as a function of penetration depth into the layer, with reported values falling in the range between 0.6 and 0.8. The current CALIPSO data processing scheme uses $\eta = 0.6$ in the analysis of cirrus clouds [*Young and Vaughan*, 2009; *Josset et al.*, 2012].

[29] Because the CPL footprint is small with respect to the mean free path of most cirrus clouds, and because simulations suggest that the impact of multiple scattering on CPL measurements is negligible [*McGill et al.*, 2002], the CPL data processing scheme assumes that $\eta$ is constant with range and equal to unity. It is understood that the use of a constant $\eta$ value for those lidar geometries (e.g., CPL) where the multiple-scattering contribution is a strong function of the cloud particle size and extinction coefficient can lead to retrieval errors. However, previous work allows us to assess the likely magnitude of these errors. Multiple scattering studies using the University of Wisconsin High Spectral Resolution Lidar [*Piironen and Eloranta*, 1994], which has a geometry similar to CPL, demonstrated that the multiple-scattering contribution to the measurement of layer optical depth via the signal loss technique may lead to underestimates of 5% or less

[*Kuehn*, 2001]. This bias is further reduced if the clear air region used to estimate the layer optical depth is 500 m or greater beyond the far side of the cloud (i.e., cloud base for down-looking system). However, the impact of multiple scattering from within the cloud being measured can be variable with penetration depth [see *Holz*, 2002, section 6], with higher $\eta$ near cloud top.

### 3.1.4. Differences in Horizontally Oriented Ice Crystal Effects

[30] In certain well-defined cases, slight differences in lidar viewing geometry can result in substantial differences in the magnitudes of the backscatter and depolarization measurements. For zenith-pointing ground-based lidars and nadir-pointing airborne and space-based lidars, specular reflection of laser light from horizontally oriented ice (HOI) crystals can generate exceptionally strong attenuated backscatter signals for which the volume depolarization ratio is essentially zero [*Platt*, 1978]. Only a slight tilt of the lidar is required to greatly diminish the anomalous attenuated backscatter signal, while simultaneously increasing the volume depolarization ratio to levels typically expected from clouds consisting entirely of randomly oriented ice (ROI) crystals [*Platt et al.*, 1978]. During CC-VEX in the summer of 2006, the difference in the pointing angles maintained by CPL and CALIOP was small ($\sim$1.7°), but still sufficient to cause significant differences in the backscatter and depolarization measured during simultaneous observations of clouds containing significant fractions of HOI. From the beginning of laser operations in June 2006 until the end of November 2007, excepting only two weeks in November 2006, CALIPSO maintained a fixed pointing angle of 0.3° off-nadir. The signature of oriented ice crystals is readily apparent in the CALIOP measurements acquired during this time [e.g., *Hu et al.*, 2007; *Noel and Chepfer*, 2010]. CPL measurements, however, are largely insensitive to the presence of HOI. This is because the ER-2 typically maintains a 2° nose-up pitch during data acquisition flights and thus only a very small fraction of the specular reflections from HOI are backscattered into the CPL field-of-view.

[31] The angular dependence of laser backscatter from HOI has direct effects on the estimates of cloud optical properties that are subsequently derived from the measurements. For nadir pointing instruments such as CALIOP, the lidar ratios for HOI clouds can approach 1 sr, as the extinction is dominated almost entirely by 180° backscatter [*Hu*, 2007]. Application of a ROI lidar ratio inside HOI clouds can have deleterious effects on extinction retrievals that use near-nadir measurements. For example, *Mioche et al.* [2010] show that CALIOP retrievals using a fixed lidar ratio of 25 sr can overestimate the extinction coefficients and optical depths in clouds containing some fraction of horizontally aligned crystals by a factor of 2 or more. The CALIOP analysis scheme identifies cloud thermodynamic phase as ROI, HOI, water, or unknown [*Hu et al.*, 2009]. As the CPL data products do not provide an explicit cloud phase classification, the cloud ice-water phase for collocated measurements is assumed to be correctly identified by the CALIOP ice-water phase algorithm.

### 3.2. Differences in Retrieval Algorithms

[32] There are several fundamental similarities and differences between the CALIOP and CPL extinction retrieval algorithms that have a large impact in comparing optical properties retrieved by the two instruments. The algorithms differ substantially for totally attenuating clouds. Highlights of the CPL algorithm and definitions of the lidar ratio categories are discussed in section 2. Complete details of the CALIOP extinction retrieval are given by *Young and Vaughan* [2009] and *Winker et al.* [2009].

### 3.2.1. Default Lidar Ratios

[33] The default values of the lidar ratio for analysis of CALIOP data are 25 sr for cirrus and 19 sr for water clouds, and are combined with a range-independent multiple-scattering correction value of 0.6 in both cases. These values are used as the initial values in all retrievals, constrained, unconstrained (default) and in totally attenuating (opaque) clouds. The default lidar ratio values for the CPL analysis rely on simple relationships between layer integrated depolarization ratio and layer average temperature (see section 2.2), resulting in values for ice clouds that are very comparable to the CALIOP default. The CPL multiple scattering correction value is set to unity.

### 3.2.2. Constrained Retrievals

[34] For extinction retrievals that can be constrained by an estimate of the layer effective optical depth, both CALIOP and CPL use essentially the same algorithm. The retrieval is performed so that the integrated profile of retrieved particulate extinction matches the constraint to within some tolerance.

[35] The main reason for differences in the retrievals from the CPL and CALIOP in these cases is the use of a different constraint. The CPL procedure, with its better SNR, can make more accurate measurements of the effective transmittance, and hence optical depth, of the layer by comparing the signals from the clear air above and below the layer [*Young*, 1995] and this value may differ from the corresponding value determined by the CALIOP analysis, especially if the layer is not the first layer sensed. The CPL analysis invokes looser tolerances to determine acceptable retrievals that may show up as more spread in the CPL constrained histograms compared to CALIOP.

### 3.2.3. Modified Default Lidar Ratio

[36] For CALIOP analyses, all retrievals are initialized with the default lidar ratio. However, if an unconstrained retrieval starts to diverge in the positive direction, then the retrieval is terminated and restarted from the top of the layer using a lidar ratio that has been reduced from the default value. Conversely, if the particulate backscatter retrieval starts to diverge in the negative direction, the retrieval is restarted with an increased lidar ratio [*Young and Vaughan*, 2009]. The CPL analysis uses a similar approach, but only invokes the modifications for divergence in the positive direction beyond set thresholds. If negative excursions of particulate backscatter beyond set tolerances appear, the optical processing for the layer is flagged as invalid.

### 3.2.4. Opaque Clouds

[37] The main difference in the retrieval algorithms used by CALIOP and the CPL occurs in the analyses of signals from totally attenuating or opaque clouds. CALIOP retrieves extinction in opaque layers using the procedure described in the previous section, although because retrievals in layers of high optical depth are extremely sensitive to the lidar ratio, the lidar ratio tends to be adjusted more often in opaque clouds than in transparent clouds.

[38] The algorithm for the CPL is quite different. In CPL data processing, opaque layers are treated as special cases of the constrained lidar ratio algorithm as discussed in section 2.2.

## 4.  Assessment of CALIOP Cirrus Optical Properties

[39] During CC-VEX, the payload of the high altitude ER-2 included the CPL, the Cloud Radar System (CRS) [*Li et al.*, 2004], the MODIS Airborne Simulator (MAS) [*King et al.*, 1996], and a visible camera. The mission was based out of Robins Air Force Base in Warner-Robins, Georgia to allow flights over ocean, subtropical cirrus, and convective anvils. A total of 10 flights had useful coincident data sets, 4 of which were at night to permit analysis of night versus day performance. The validation procedure implemented for the NASA ER-2 aircraft was to fly the predicted ground track of CALIPSO for 30 to 40 min centered on the predicted overpass time. Refer to *Yorks et al.* [2011b] for details of the ten coincident segments. To achieve a balance between having enough data points and restricting the analysis close to the exact coincidence, comparisons in this paper use data segments that are two degrees latitude in length and centered at the exact coincident second for each of the ten flights.

### 4.1.  Statistical Methods

[40] The validation results presented here use Version 3.01 of the CALIOP Level 2 cloud data products. The CALIOP parameters used in the analyses are: (1) cloud layer lidar ratios at 532 nm, which are reported at 5 km horizontal resolution in the CALIOP 5 km cloud layer product; (2) cloud layer average temperatures at 5 km horizontal resolution, which are computed from data provided in the CALIOP 5 km cloud profile product; (3) cloud layer opacity flags, lidar ratio flags, ice water phase flags, and extinction QC flags at 5 km horizontal resolution, all of which are extracted directly from the 5 km cloud layer products; and (4) 532 nm cloud extinction profiles, which are reported in the cloud profile product at horizontal resolution of 5 km and vertical resolution of 60 m.

[41] The CPL analysis produces similar standard products, but at a finer resolution. A procedure was developed to match each standard 5 km along-track CALIOP data profile with CPL data points (bins) by averaging the appropriate cluster of CPL attenuated backscatter values. CPL layer boundaries, lidar ratios, and extinction profiles are then calculated from the new lower resolution backscatter results. The CALIOP resolution results in 47 coincident 5 km profiles on average per coincident segment. If the ER-2 travels the segment in the opposite direction of the CALIPSO track, the CPL profile assignments are adjusted accordingly. The results of this procedure, after all ten flights were processed and merged, were one CPL data file and one CALIOP data file containing all pertinent Level 2 parameters co-aligned bin-to-bin. By using these co-aligned files, statistics could be derived and compared on a bin-to-bin basis.

[42] Based on the above data sets, two statistical methods were employed for this study. Method 1 is a compilation showing lidar ratio and extinction distributions for all CPL cloud bins and all CALIOP cloud bins found independently

above 8 km and restricted to various lidar ratio or diurnal categories in all the coincident segments. This includes bins where CPL data is in a cloud but CALIOP is not and vice versa. In its basic form, this method does not restrict the data set based on ice particle orientation. To develop histograms where the data sets are restricted to HOI or ROI conditions, this method is necessarily restricted to inside CALIOP layers because the CPL data products do not provide an explicit ice orientation classification. Method 2 is subset of Method 1 with higher restrictions. These bin-to-bin comparisons involve all in-cloud coincident pairs where both instruments have positive extinction (i.e., both inside clouds), both are in the same lidar ratio and diurnal category, and cloud temperatures are less than or equal to −15C. We have further restricted the data set to ROI conditions for this method.

### 4.2.  CC-VEX Case Studies

[43] Two coincident segments are highlighted, one in the daytime and one at night, to visualize the differences in coincident input backscatter signals and resultant optical retrievals between CPL and CALIOP. Figure 4 illustrates the attenuated backscatter for the daytime case of 31 July 2006. The coincident segment was just east of the Yucatan Peninsula in the Caribbean Sea with the point of closest coincidence at 19:16:30 UTC near the coordinates 18.3143 North and 86.0125 West and with a ground track separation of 556 m. Figure 4a displays the native high resolution CPL signals with 200 m horizontal resolution to compare with the averaged 5 km resolution CPL signals in Figure 4b and the averaged 5 km resolution CALIOP signals in Figure 4c that were used for input into the optical properties algorithms. The better SNR in the CPL data is apparent in comparing Figures 4b and 4c. So too is the fact that the two instruments are sensing different cloud scenes at the beginning of the segment when CPL was 10 min earlier in time compared with CALIOP. Other than the discrepancies above, the attenuated backscatter data of CALIOP compare favorably to CPL with only localized exceptions. Figure 5 shows the extinction retrievals corresponding to Figure 4. In general, the 5 km extinction values, which are color-coded on a log scale, illustrate good agreement except where the two lidars are likely sensing different clouds (e.g., between 17.25 and 17.60 N latitude) and at other scattered localized areas. The 200 m resolution CPL extinction retrieval (Figure 5a) displays some details that the others miss when they average to 5 km. Figure 6 illustrates CPL and CALIOP column optical depth retrievals for this coincident segment for the vertical zone 18–8 km. The high resolution (200 m) CPL retrieval is shown in green with 5 km resolution retrievals shown is in blue (CALIOP) and red (CPL). The two shaded boxes show areas where the lowest detected layer was intermittently opaque. Optical depth is calculated using Method 1 with no filtering. Since most of the layers in the segment are transparent and the CALIOP data is averaged to 5 km or more to overcome lower SNR, there is generally good agreement between the two instrument data sets at the 5 km horizontal resolution. The scattered instances of higher CALIOP optical depth between 17.6 degrees and 17.9 degrees north can be traced back to specific small clouds that had larger backscatter signals and retrieved extinction from CALIOP compared to CPL.
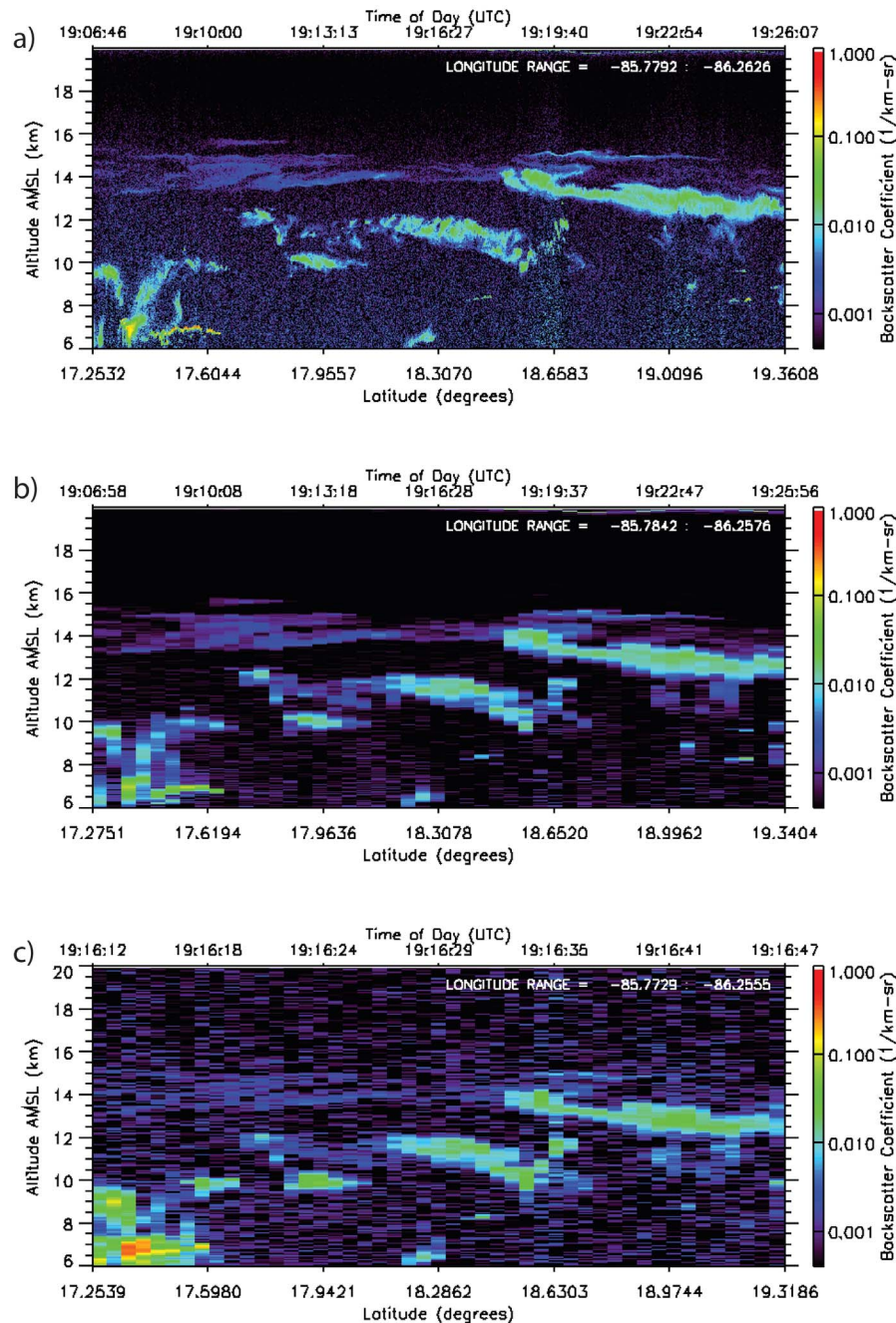
**Figure 4.** CPL and CALIOP calibrated total attenuated backscatter used as input into optical processing for the 31 July 2006 daytime coincident segment. (a) The 200 m resolution CPL data, (b) the 5 km resolution CPL data, and (c) the 5 km resolution CALIOP data. The aircraft and satellite were at the closest point in space and time at 19:16:30 UTC.

[44] Figure 7 shows the attenuated backscatter for the nighttime case of 11 August 2006 displayed in the same fashion as Figure 4. The coincident segment was centered in Kentucky with the point of closest coincidence at 08:00:00 UTC near the coordinates 37.2434 N and 87.8329 W with a ground track separation of 498 m. The better SNR in the nighttime data is readily apparent, especially with CALIOP data, compared to the daytime case (Figure 4). In general, signal strengths compare favorably. The right third of this coincident segment is dominated by opaque clouds and one manifestation of this is deeper penetration by the CALIOP lidar caused by multiple scattering [*Yorks et al.*, 2011b]. Figure 8 displays the corresponding extinction retrievals in the same fashion as Figure 5. In general, the 5 km extinction values for the left two thirds of the panels demonstrate good agreement, where transparent clouds were detected by both instruments. Similarly, the column optical depth retrievals for the vertical zone 18–8 km (Figure 9) are also in good agreement in this region of the coincident segment. There is a region just to the left of the
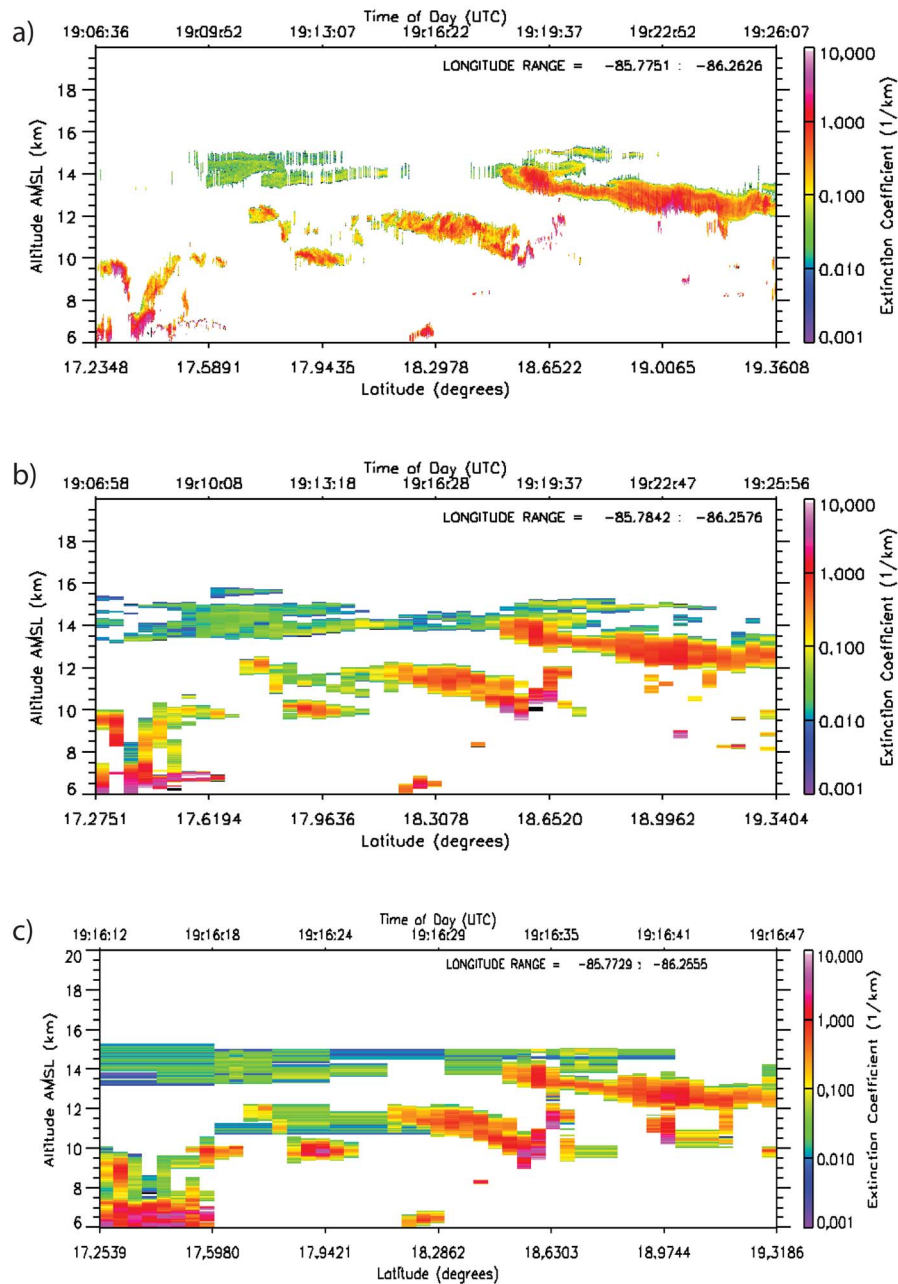
**Figure 5.** CPL and CALIOP extinction retrievals are shown for the 31 July 2006 daytime coincident segment. (a) The full 200 m resolution CPL data, (b) the 5 km resolution CPL data, and (c) the 5 km resolution CALIOP data.

shaded area in Figure 9 that has higher CALIOP retrievals. Here the CALIOP layer algorithm combined with stronger multiple scattering has detected more in-cloud bins below the main body of the cloud, resulting in an area of higher CALIOP optical depth. However, in the opaque cloud in the right portion of the segment, the 5 km CPL extinction coefficients in Figure 8 are greater than the 5 km CALIOP extinction, especially near cloud base. Similarly the optical depths are higher for CPL in the shaded opaque area of Figure 9. The disparity is a result of the differing penetration distances and differing opaque algorithms discussed in section 3.2.4 and this case is a very good example of the disagreement inside the penetrated portion of opaque cirrus layers, an issue that will be discussed throughout the paper. It should be stressed that neither lidar is penetrating the full physical depth of the opaque cloud layer and that, consequently, neither lidar is measuring the total optical depth of the cloud.

### 4.3.  CC-VEX Lidar Ratio Statistics

[45]  Unlike extinction, which is retrieved bin-by-bin in profiles, lidar ratios are specified by atmospheric layer for both instruments. For the CALIOP co-aligned data set, the lidar ratio and extinction quality control (QC) flag
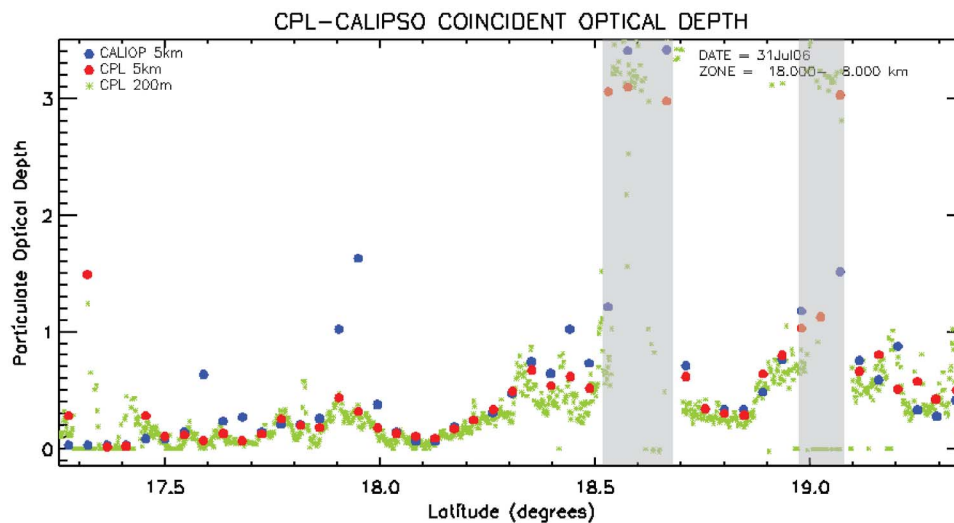
**Figure 6.** CPL and CALIOP column optical depth retrievals during the 31 July 2006 coincident segment for the vertical zone 18–8 km. High resolution CPL retrievals are shown in green with 5 km resolution CALIOP retrievals shown in blue and 5 km CPL retrievals shown in red. The two gray boxes show areas where the last layer sensed was intermittently opaque. Optical depth is calculated using Method 1 with horizontal oriented ice crystals included.

information were remapped into profiles matching the extinction profile from the 5 km product (5 km by 60 m) by using the top and bottom vertical bin locations of the layer. The CPL lidar ratios and lidar ratio QC flags were remapped similarly for the CPL co-aligned data set. In this section, we will compare the lidar ratios used by the two instruments, discuss the similarities and differences observed during the ten coincident CALIPSO overpass segments from the CC-VEX campaign, and discuss the impacts of any discrepancies in the two data sets. All lidar ratio statistics refer to the true lidar ratios (i.e., those that have been corrected for multiple scattering).

[46] Using Method 1, Table 2 displays the ice cloud diurnal distribution in this study along with the percentage of detected HOI using the CALIOP analysis. The CPL daytime cloud contribution is 45%, with 55% at night. CALIOP data has a higher percentage of clouds at night (61%). This is consistent with the findings by *Yorks et al.* [2011b] where it was demonstrated during CC-VEX coincident segments that the number of daytime cloudy bins was about the same between the two instruments, but the CALIOP analysis found many more cloudy bins at night. As defined in section 2.2, the lidar ratio can be assigned to four categories: constrained, default, modified default, and opaque. Initial unfiltered statistics for the various lidar ratio categories are shown in Table 3 using Method 1. The last two rows of Table 3 tabulate the average lidar ratio implemented during CC-VEX for each instrument for each of the categories plus the overall average. A total of 13249 in-cloud bins were observed by CPL and 17111 by CALIOP. CPL data was found to have a higher overall average lidar ratio at 25.4 sr compared to CALIOP at 23.5 sr. (Using the more restrictive Method 2, the CPL lidar ratio average was 25.8 sr compared to CALIOP at 24.6 sr.) Constrained lidar ratios, where the lidar ratios have fewer assumptions made during optical calculations, represent 32% of CPL cloud bins and only 13% of CALIOP cloud bins. This can be

attributed to the better SNR in the input CPL attenuated backscatter. CPL data averages 26.8 sr for constrained lidar ratios while CALIOP data averages 25.0 sr, which is a small contributing factor to the higher overall CPL average. During the CC-VEX campaign, CALIOP processing did not detect any daytime transparent cirrus that met the quality assurance requirements for constrained retrievals. In the default category, which has the most observations, the lidar ratios of both instruments are about 25, but the CALIOP data has almost twice as many occurrences. This category represents 42% of CPL cloud bins and 56% of CALIOP cloud bins. The modified default category is a minor contributor to the overall statistics because of the number of observations (5% of both CPL and CALIOP data sets) despite the fact that the CALIOP average value is nearly 5 sr higher than the CPL average. This difference is due to the fact that CPL analysis only modifies the default ratio downward while the CALIOP analysis can modify up or down.

[47] The initial unfiltered statistics for opaque layers show the average CPL and CALIOP lidar ratios are 25.8 sr and 20.0 sr respectively (Table 3), due to algorithm differences and the effects of the lower SNR in CALIOP signals. The more filtered results from Method 2 displayed in Table 4 yield a CPL lidar ratio average of 28.3 sr compared to CALIOP at 24.1 sr. These lidar ratio differences in the penetrated portions of opaque clouds contribute significantly to the difference in overall lidar ratios between the two instruments. Opaque layers represent 21% of the CPL data set and 26% of the CALIOP data set. For both instruments, opaque layers are reported in the data products using QC flags. To isolate the opaque algorithm influence, we developed histograms for opaque layers with randomly oriented ice (ROI) particles (not shown). CPL lidar ratios averaged 27.9 sr while CALIOP averaged 23.7 sr. This discrepancy in the lidar ratio significantly influences extinction retrievals (discussed in sections 4.2 and 4.4) because the particulate transmittance squared term is approaching zero in opaque
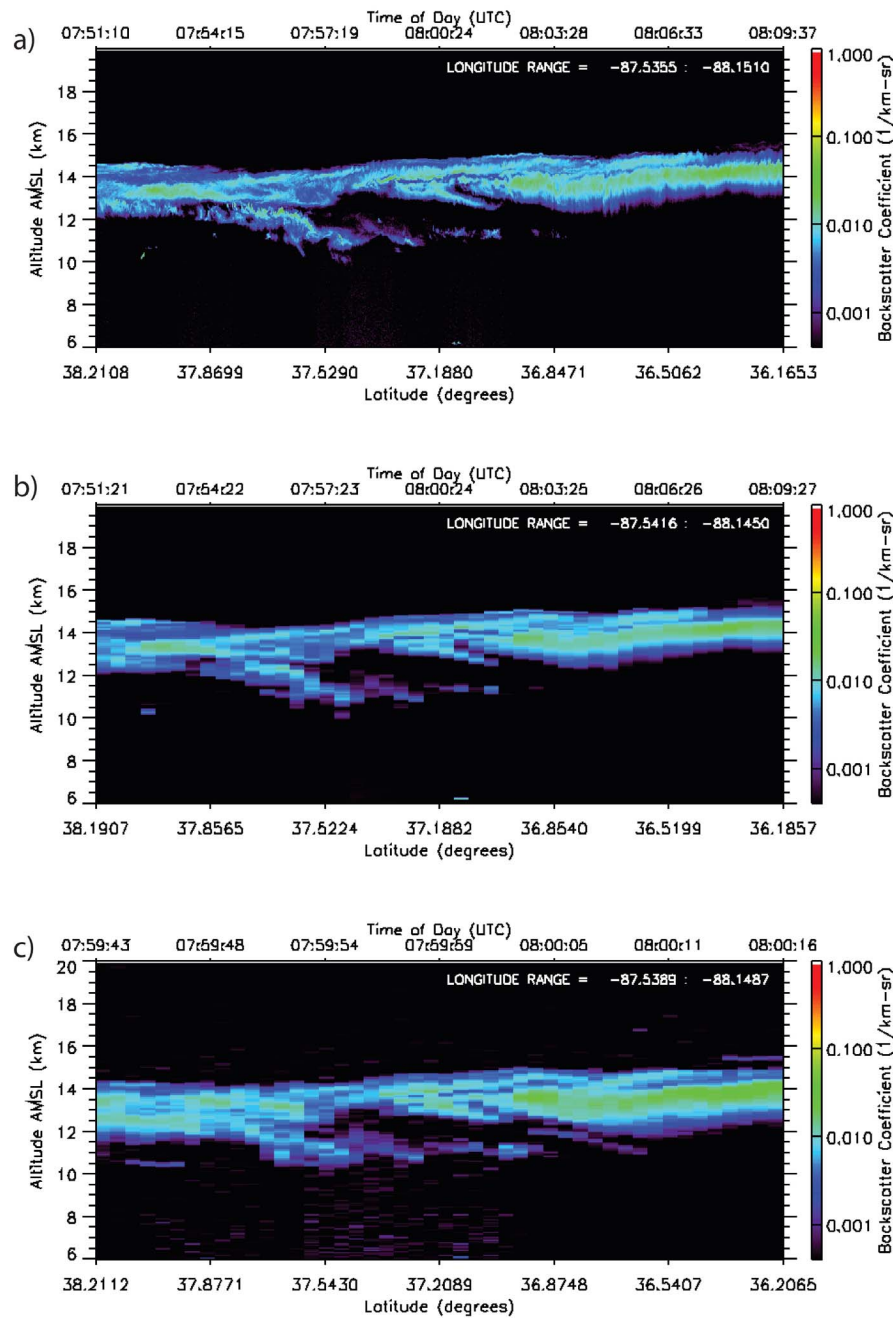
**Figure 7.** CPL and CALIOP calibrated total attenuated backscatter used as input into optical processing for the 11 August 2006 nighttime coincident segment. (a) The 200 m resolution CPL data, (b) the 5 km resolution CPL data, and (c) the 5 km resolution CALIOP data. The aircraft and satellite were at the closest point in space and time at 08:00:00 UTC.

clouds and the lidar equation result becomes highly nonlinear.

[48] The CALIOP data set during CC-VEX demonstrated a HOI frequency of 15%. The impact of HOI conditions during CC-VEX is shown in the lidar ratio histograms of Figure 10 using a frequency bin size of 4 sr. Figure 10a illustrates the influence HOI has on CALIOP lidar ratio retrievals (black plot), causing more frequent low values, resulting in an average lidar ratio for HOI of 16.6 sr compared with 24.9 sr for ROI (green plot), although the main modal values are identical. CPL views further off-nadir than does CALIOP, resulting in smaller HOI influence, as shown in Figure 10b. For CPL under HOI conditions (black plot), the resulting average lidar ratio is 23.9 sr compared with 25.8 sr for ROI (red plot). The two instruments compare well under the randomly oriented ice conditions in Figure 10. The histograms in Figure 10 include both transparent and opaque conditions. For transparent conditions only, the average CALIOP value for HOI conditions is 21.5 sr while the average for ROI conditions is 25.2 sr. The CPL values are
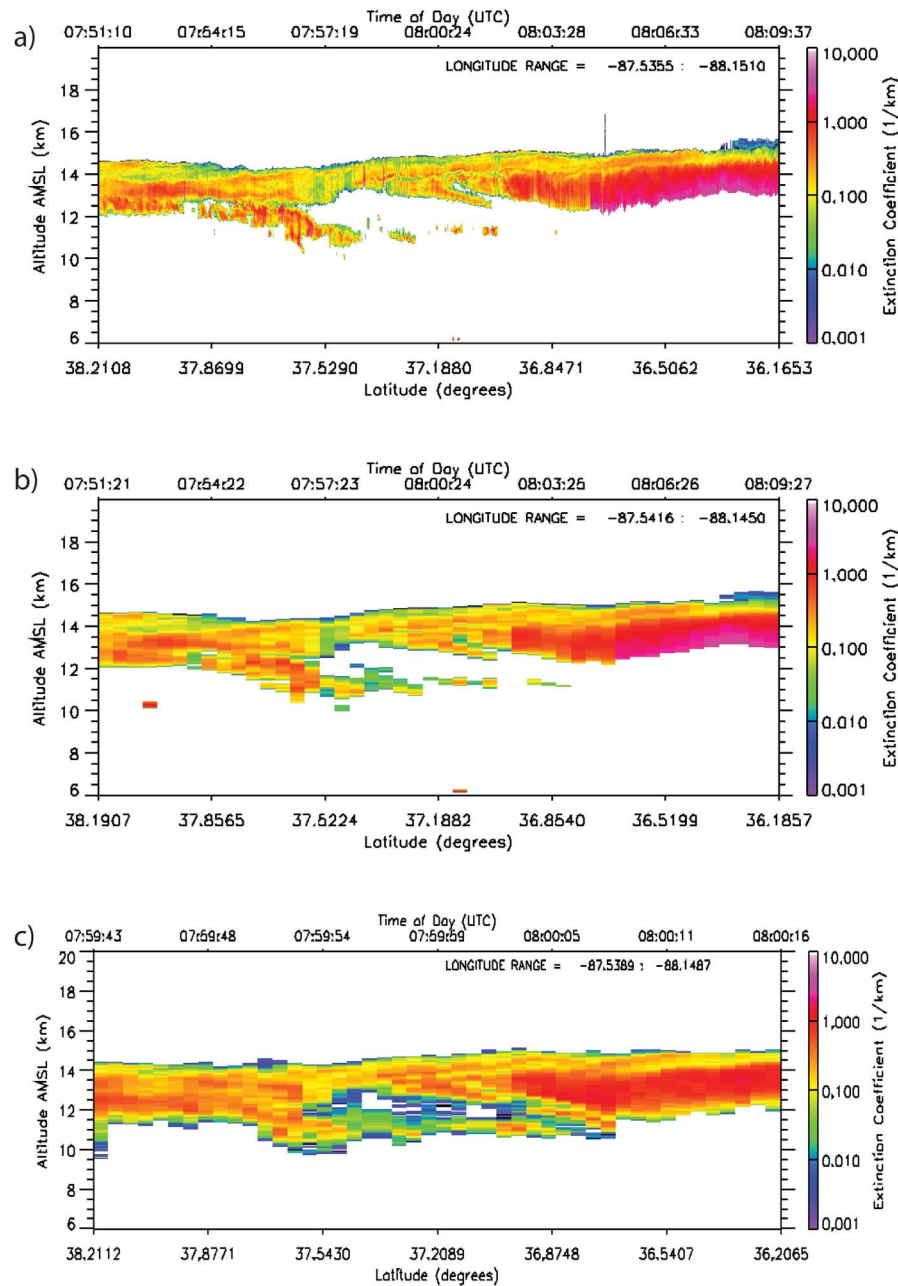
**Figure 8.** CPL and CALIOP extinction retrievals are shown for the 11 August 2006 nighttime coincident segment. (a) The full 200 m resolution CPL data, (b) the 5 km resolution CPL data, and (c) the 5 km resolution CALIOP data.

24.8 sr and 25.3 sr, respectively, showing the smaller influence. The resultant CALIOP extinctions in HOI conditions are impacted to a smaller degree because of the compensation by the abnormally strong backscatter found during HOI situations. This is discussed in section 4.4. The discrepancies between the two instruments are magnified during conditions that are both HOI and opaque. Here CPL lidar ratios average 22.6 sr and CALIOP averages 13.4 sr, consistent with the expectations discussed earlier in section 3.1.4. Sixty percent of HOI conditions are found during opaque layers. Based on these results for HOI and opaque cloud layers, the authors believe the more meaningful statistics for CALIOP

lidar ratio validation are for the subset of the data that filters out the HOI and opaque conditions by using the various available flags.

[49] Distributions of the lidar ratio for the subset of transparent ROI conditions using Method 1 are shown in Figure 11, which also uses a frequency bin size of 4 sr. The CPL distributions are in red and the CALIOP distributions are in blue. The mean lidar ratio of CPL (25.3 sr) and CALIOP (25.2 sr) as well as the distribution of lidar ratio for both instruments, are in good agreement for all layers (Figure 11a). Also, the more filtered lidar ratio statistics using Method 2 are reported in Table 4. For all transparent
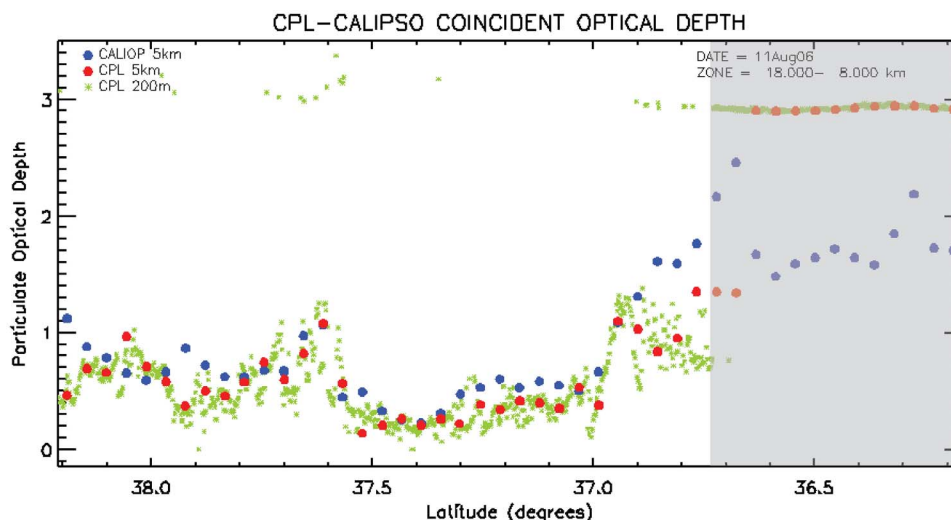
**Figure 9.** CPL and CALIOP column optical depth retrievals during the 11 August 2006 coincident segment for the vertical zone 18–8 km. High resolution CPL retrievals are shown in green with 5 km resolution CALIOP retrievals shown is in blue and 5 km CPL retrievals shown in red. The gray box designates an area where the last layer sensed is opaque. Optical depth is calculated using Method 1 with horizontally oriented ice crystals included.

layer data points, which comprise 77% of the data in Table 4, CALIOP lidar ratios average just 2.1% lower than CPL, with an RMS difference of 9.9 sr. In the daytime, a large percentage of the cloud bins use the default lidar ratio, with CPL data at 64% and CALIOP data at 59% (Table 3). Figure 11b displays the daytime transparent ROI histograms, with good agreement in the distributions of both instruments. The CPL mean lidar ratio is 25.5 sr, higher than CALIOP (23.9 sr), but the modes are identical. Using Method 2, Table 4 shows the daytime mean lidar ratio of both instruments slightly increases, yielding a relative difference of −7.6% (CALIOP-CPL). The low SNR during the daytime inhibits CALIOP constrained lidar ratios. However, since CPL data has better SNR, it is able to calculate constrained ratios 7% of the time. These CPL daytime constrained values contribute to the higher mean lidar ratio during the daytime.

[50] At night, the most frequent lidar ratio category in the CALIOP data remains the unmodified default (at 53%) but now 22% of the cloud bins are in the constrained category. For CPL at night, a large shift away from unmodified default (now 24%) to constrained (53%) occurs. Figure 11c illustrates the good agreement between both instruments for the nighttime transparent ROI lidar ratio histograms. Furthermore, CPL nighttime mean lidar ratio is 25.2 sr and CALIOP nighttime mean lidar ratio is 25.9 sr. For Method 2, the mean lidar ratios also agree well, with the CALIOP average slightly higher, resulting in a relative difference of 1.2%. We also compared the distribution of the constrained lidar ratio category at night under ROI conditions in Figure 11d. CPL data has a noticeably lower mode (21 sr) compared to CALIOP data (24.5 sr). However, the mean lidar ratios compare favorably, with CPL at 25.2 sr and CALIOP at 24.9 sr due to the more abundant high outliers in the CPL distribution. Using Method 2, the CPL mean constrained lidar ratio decreases to 22.0 sr, (see Table 4) close to the mode value of Figure 11d. This smaller average CPL lidar

ratio likely stems from the more restrictive filtering used in Method 2. Constrained CPL bins paired with non-constrained CALIOP bins that were used in calculating Method 1 CPL averages are no longer used in Method 2, which would eliminate some of the thin cirrus in the CPL data set that tend to have higher lidar ratio outliers. As evidence, further analysis demonstrates that the data group eliminated in the CPL data set going from Method 1 to Method 2 has an average extinction of 0.152 compared to 0.251 using Method 2. Comparing constrained lidar ratios in an exact bin-to-bin analysis is also complicated by the possibility that different boundary conditions may be used in the retrievals by CALIOP and CPL in the case of layers that are beneath other layers. These boundary values include the correction for the attenuation by overlying layers, which may cause differences in the constrained lidar ratios between each instrument.

### 4.4. CC-VEX Extinction and Optical Depth Statistics

[51] As discussed in sections 3 and 4.3, uncertainties in the attenuated backscatter and lidar ratio will have a direct effect on extinction retrievals. CALIOP extinction statistics formulated using Method 1 without any filtering averaged 22.2% below CPL statistics (20.8% below using Method 2). The cause of most of the reduced CALIOP values has been traced to opaque cloud conditions, where CALIOP extinction averaged almost 46% below CPL values (see Table 5). Figure 1b demonstrates the effect of the lidar ratio discrepancy on opaque layer extinction retrievals using Method 2.

**Table 2.** Diurnal Distribution of Ice Clouds in Coincident Segments of CC-VEX

|  | Day CPL | Day CALIOP | Night CPL | Night CALIOP | HOI CALIOP |
|---|---|---|---|---|---|
| Percent of Total | 45 | 39 | 55 | 61 | 15 |

**Table 3.** Lidar Ratio Distributions for Ice Clouds in Coincident Segments of CC-VEX Using Method 1

| | Lidar Ratio Category | | | | |
| --- | --- | --- | --- | --- | --- |
| | All | Constrained | Unmodified Default | Modified Default | Opaque Layers |
| Number of Observations (CPL) | 13249 | 4244 | 5534 | 664 | 2807 |
| Number of Observations (CALIOP) | 17111 | 2312 | 9533 | 775 | 4491 |
| All CPL (% of Total) | 100 | 32 | 42 | 05 | 21 |
| All CALIOP (% of Total) | 100 | 13 | 56 | 05 | 26 |
| Day CPL (% of Total) | 100 | 07 | 64 | 10 | 19 |
| Day CALIOP (% of Total) | 100 | 00 | 59 | 11 | 30 |
| Night CPL (% of Total) | 100 | 53 | 24 | 01 | 22 |
| Night CALIOP (% of Total) | 100 | 22 | 53 | 01 | 24 |
| HOI CALIOP (% of Total) | 100 | 02 | 29 | 09 | 60 |
| CPL Mean Value (sr) | 25.4 | 26.8 | 25.1 | 18.1 | 25.8 |
| CALIOP Mean Value (sr) | 23.5 | 25.0 | 24.9 | 22.9 | 20.0 |

Figure 1b shows all coincident points, including those from opaque layers (circled). Opaque layers make up 17% of the Method 2 data set. The correlation coefficient improves from 0.51 to 0.65 when opaque layers are omitted.

[52] Because of the very high attenuated backscatter associated with HOI conditions, the use of default lidar ratios not lowered to reflect the conditions would result in an increase in extinction (see section 3.1.4). Figure 12a compares the extinction distribution of CALIOP data during HOI conditions (black) with the one from ROI conditions (blue). The HOI distribution shows more frequent high values compared to ROI conditions. During CC-VEX, the majority of HOI conditions were found in opaque cloud layers, so the results would also trend higher for that reason. CPL and CALIOP extinction distributions compare well under transparent HOI conditions (Figure 12b) despite the fact that the average CALIOP lidar ratio is lower. Here CALIOP data (green histogram) averages $0.52$ km$^{-1}$ and CPL data (red histogram) averages $0.48$ km$^{-1}$.

[53] To assess the impact on optical depth from the various uncertainties and discrepancies found in the CC-VEX data sets, the average column optical depth in the vertical zone between 8 and 18 km through all the coincident segments was computed by integrating all in-cloud extinction values with no filtering for opaque layers or HOI. The results are given in Table 6. For all ice clouds, CALIOP optical depth averages only 2.2% lower than CPL values despite the fact that we found the unfiltered CALIOP average extinction coefficient 22% below the CPL average. The lower extinction values of CALIOP (found mostly in opaque layers) are compensated by the nearly 4000 more cloud bins being integrated into the CALIOP data set. Many of these extra cloud bins are from the CALIOP signal's greater penetration

depth due to multiple scattering during opaque conditions and others are artifacts introduced by the CALIOP multiple resolution (5–20–80 km) layer detection scheme [*Yorks et al.*, 2011b]. Nighttime CALIOP cloud column optical depth is 10.1% lower than CPL values, while CALIOP daytime values are 6.0% higher than CPL. This matches with the extinction histograms in Figure 13 (plots b and c) plus the fact that a higher percentage of opaque layers were found during the day with CALIOP compared to CPL (Table 3). The results for CC-VEX indicate that, despite the uncertainties and discrepancies, CALIOP overall ice cloud optical depth compares favorably to CPL values due to the cancellation of opposing CALIOP effects.

[54] As with the lidar ratio analysis, the most meaningful comparison of extinction involves filtering out HOI and opaque conditions. The frequency distributions of CPL and CALIOP extinction during the 10 coincident segments using Method 1 but restricting bins to all transparent ROI conditions are displayed in Figure 13a. The CALIOP distribution (green) agrees well with CPL distribution (red) and the CALIOP mean extinction of $0.19 \pm 0.52$ km$^{-1}$ is the same as the CPL mean extinction of $0.19 \pm 0.33$ km$^{-1}$, but with a larger standard deviation. On average, CALIOP extinction for all transparent ROI layers using Method 2 is 14.7% higher than CPL values, as shown in Table 5, and the RMS difference is found to be $0.25$ km$^{-1}$. This higher average CALIOP extinction likely stems from the more restrictive filtering used in Method 2. Transparent CPL bins paired with opaque CALIOP bins that were used in Method 1 averages are no longer used in Method 2, which would tend to lower the CPL average extinction using Method 2. The category mismatch most likely comes about when a vertical cloud cluster is interpreted as multilayered by the CPL

**Table 4.** Coincident Lidar Ratio Statistics for CC-VEX Using Method 2

| Ice Cloud Category (Both Instruments) | Number of Observations {% of Total} | Average CPL Lidar Ratio (sr) | Average CALIOP Lidar Ratio (sr) | Average Relative Lidar Ratio Difference (%) | RMS Difference (sr) |
| --- | --- | --- | --- | --- | --- |
| All Bins | 9598 {100} | 25.8 | 24.6 | −4.7 | 9.5 |
| All Bins Transparent | 7405 {77} | 25.7 | 25.1 | −2.1 | 9.9 |
| Day Transparent | 2741 {28} | 26.2 | 24.2 | −7.6 | 6.8 |
| Night Transparent | 4664 {49} | 25.4 | 25.7 | 1.2 | 11.4 |
| Constrained Lidar Ratios | 1235 {13} | 22.0 | 25.2 | 14.5 | 6.2 |
| Default Lidar Ratios | 3295 {34} | 25.3 | 24.9 | −1.3 | 0.7 |
| Opaque Layers | 1622 {17} | 28.3 | 24.1 | −15.1 | 7.7 |
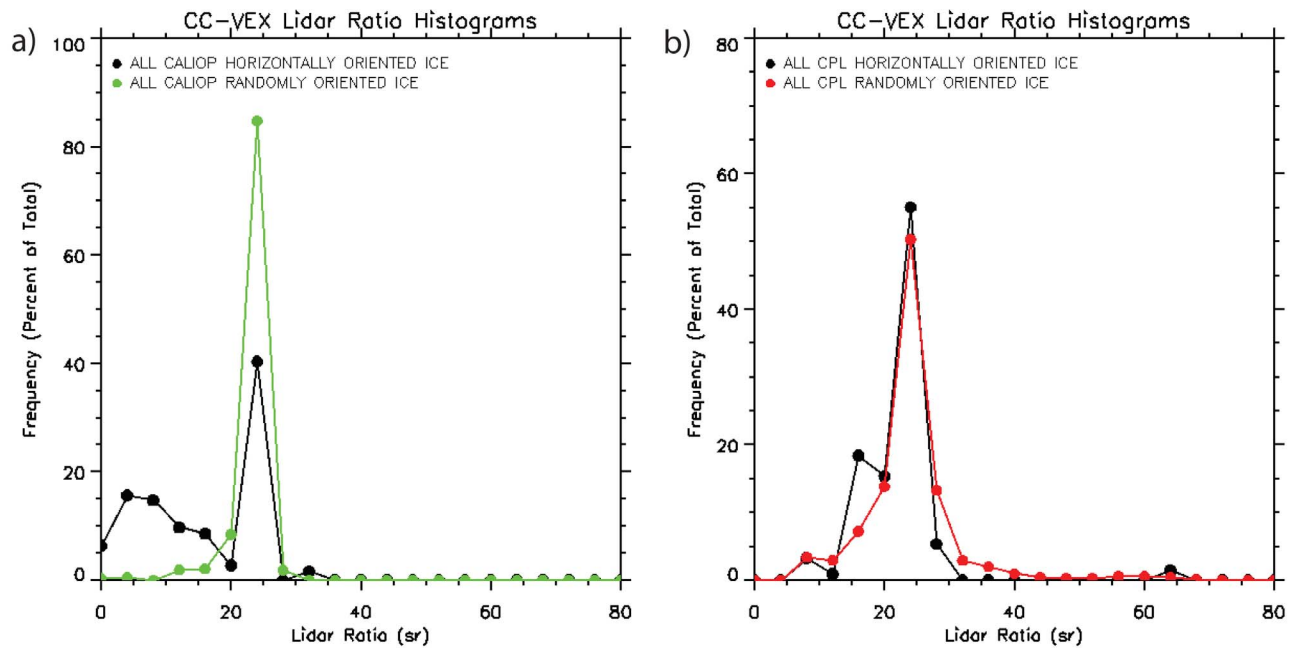
**Figure 10.** (a) The influence HOI has on the lidar ratio of CALIOP, causing more frequent low values in its HOI histogram (black) compared to the ROI histogram (green). CPL's viewing geometry is pitched at a higher angle from nadir compared to CALIOP during this study. This results in much less of an influence for (b) CPL, also showing its HOI histogram in black. The two instruments compare very well under ROI conditions (green CALIOP histogram and red CPL histogram).

procedure and single-layered by CALIOP [*Yorks et al.*, 2011b]. Another effect of the filtering in Method 2 would cause a shedding of CALIOP data points inside transparent layers paired with CPL bins not in a layer, which would tend to be the weaker values. This situation most likely comes about when the CALIOP analysis is using the lower-resolution feature finder to discover thin clouds, which tends to smear cloud locations in regions where the CPL analysis detects none [*Yorks et al.*, 2011b]. Further analysis of the joint backscatter PDF plot for transparent ROI cases (not shown) indicates this to be true. Figure 14a, which color-codes the frequency distribution of all transparent point pairs in a PDF using Method 2, shows that most of the points lie on or near the dashed line representing one-to-one correspondence. The result of the linear regression of the CALIOP and CPL data in the all transparent category (Figure 14a) is:

$$CALIOP = (0.845 \pm 0.011) * CPL + (0.05233 \pm 0.00347)$$
$$\text{with } r = 0.651. \tag{7}$$

Also, average extinction values as a function of height have been produced (not shown). As expected, the weakest extinction retrievals are above 14 km and the strongest are below 10 km. An average ice cloud column optical depth was computed by vertically integrating the extinction values using Method 2 for each profile for each instrument. Hereafter, optical depths discussed will be from this method. CPL retrieved an average optical depth for all transparent ROI clouds of 0.29, which is 0.04 lower than the average CALIOP optical depth.

[55] CALIOP daytime retrievals are also compared with CPL retrievals inside transparent ROI conditions using Method 1. CALIOP average daytime extinction is 0.03 km$^{-1}$ higher than CPL values, but the shapes of the extinction frequency distributions of both instruments are similar (Figure 13b). The standard deviation is 0.32 km$^{-1}$ higher for CALIOP. The joint CPL-CALIOP extinction PDF for daytime conditions using Method 2 (Figure 14b) shows a relatively wide spread and a correlation coefficient of 0.610, lowest of the four panels. Here, the average CALIOP extinction is 0.02 km$^{-1}$ higher, with an RMS difference of 0.35 km$^{-1}$. CPL average column optical depth for transparent daytime conditions is 0.25, 0.03 lower than CALIOP. The disagreement between the two instruments for daytime conditions reflects the noisier conditions with solar background during the day, despite the fact that both instruments use similar lidar ratios frequently during daytime hours. The noise causes additional uncertainty in the daytime attenuated backscatter values and this uncertainty dominates the extinction retrievals.

[56] Nighttime transparent ROI CALIOP extinction retrievals agree well with CPL retrievals, except for the more frequent low values for CALIOP. This tendency for CALIOP allows the CPL average extinction using Method 1 to be 0.01 km$^{-1}$ higher compared with CALIOP and the CPL data to have less spread in the extinction frequency distribution (Figure 13c). The tendency for CALIOP to have more frequent lower values using Method 1 is likely due to the smearing of CALIOP cloud locations in regions where the CPL analysis detects none [*Yorks et al.*, 2011b]. CPL and CALIOP standard deviations are at their lowest at night,
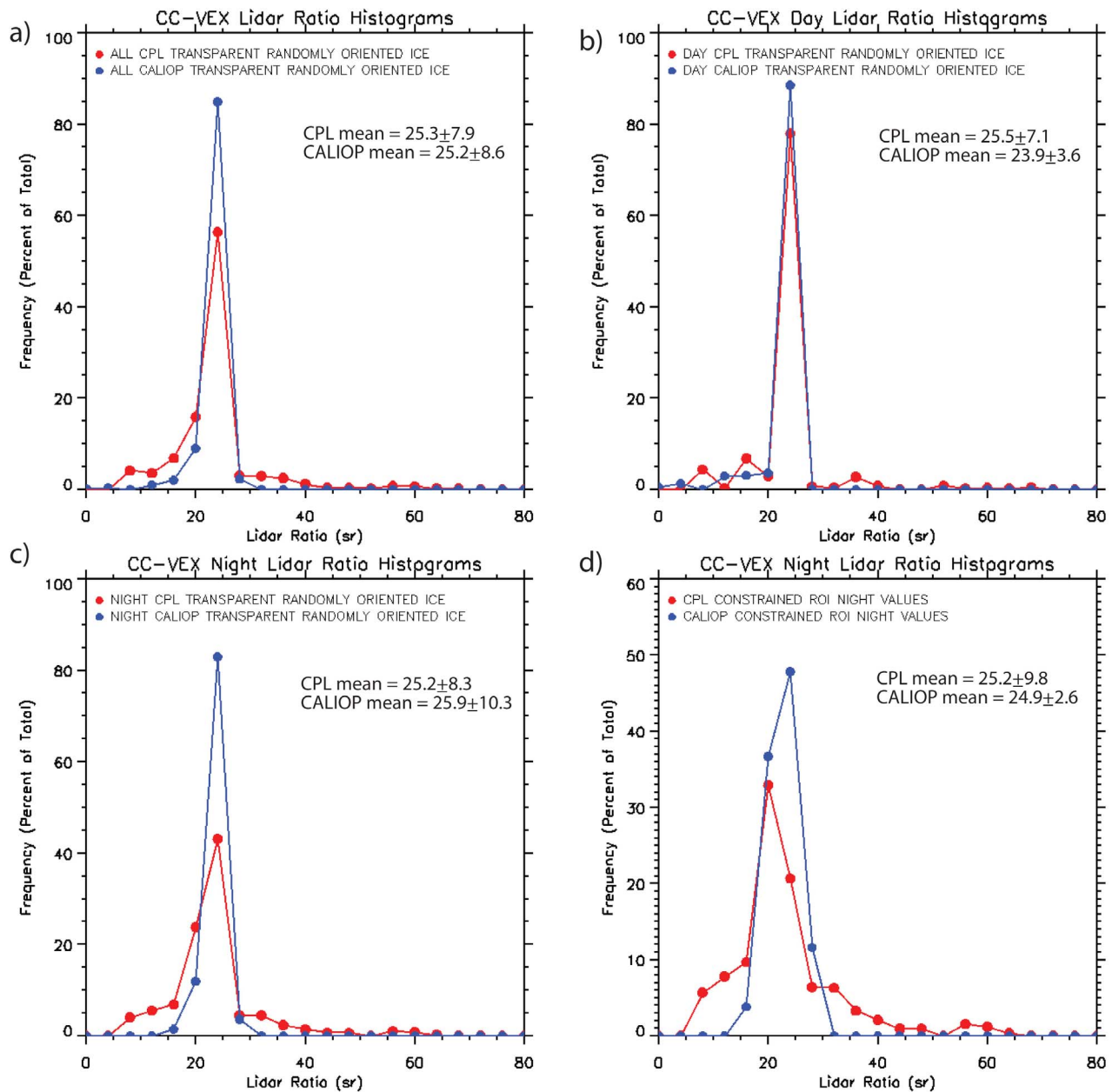
**Figure 11.** CPL (red) and CALIOP (blue) lidar ratio frequency distributions during CC-VEX coincident segments restricted to transparent ROI conditions only. (a) The overall distribution, (b) the daytime distribution, (c) the full nighttime distribution, and (d) shows the nighttime constrained distribution.

as expected. The restrictions in place using Method 2 alter this comparison. The joint PDF for night transparent cases is displayed in Figure 14c using Method 2. As expected, the night transparent correlation coefficient (0.736) is better than daytime conditions (Table 5), but CALIOP extinction is 16.5% higher on average in Figure 14c compared with the corresponding values from CPL. Also, the RMS difference is low at 0.15 $km^{-1}$ with the higher SNR at night. Finally, CPL nighttime column optical depth averaged 0.32 while CALIOP data was 0.05 higher using Method 2. For nighttime cases, both instruments use a mix of default and constrained lidar ratios, with the CPL data having a much larger percentage of constrained. Extinction retrieval histograms using

Method 1 for nighttime constrained lidar ratios are illustrated in Figure 13d. CALIOP values averages 0.05 $km^{-1}$ more than CPL values with the mode also higher. Using Method 2, Figure 14d shows the joint extinction PDF for nighttime constrained lidar ratios. There is a one-to-one correspondence in the slope of the linear fit (not shown), but it has an offset of 0.078 $km^{-1}$. This offset results in an average relative difference of +30.8% in CALIOP extinction values compared to CPL with a correlation coefficient of 0.755. This is a direct result of the use of different optical depth constraints for CALIOP compared to CPL during coincident constrained conditions, resulting in different lidar ratio values being used.

**Table 5.** Coincident Extinction Statistics for CC-VEX Using Method 2

| Ice Cloud Category (Both Instruments) | Average CPL Extinction (km$^{-1}$) | Average CALIOP Extinction (km$^{-1}$) | Average Relative Extinction Difference (%) | RMS Difference (km$^{-1}$) | Correlation Coefficient |
|---|---|---|---|---|---|
| All Bins | 0.397 | 0.314 | −20.8 | 0.692 | 0.513 |
| All Bins Transparent | 0.173 | 0.199 | 14.7 | 0.247 | 0.651 |
| Day Transparent | 0.196 | 0.220 | 12.2 | 0.354 | 0.610 |
| Night Transparent | 0.160 | 0.186 | 16.5 | 0.154 | 0.736 |
| Constrained Lidar Ratios | 0.251 | 0.329 | 30.8 | 0.216 | 0.755 |
| Default Lidar Ratios | 0.141 | 0.152 | 7.4 | 0.145 | 0.804 |
| Opaque Layers | 1.281 | 0.695 | −45.8 | 1.125 | 0.499 |

Column optical depth during constrained lidar ratio conditions is 0.64 for CPL data and 0.84 for CALIOP data.

[57] The best agreement in extinction between the two instruments occurs for transparent ROI layers using a default lidar ratio (day and night), displayed in Table 5. CALIOP extinction is only 7.4% higher than CPL values and the RMS difference is calculated to be 0.15 km$^{-1}$ with a correlation coefficient of 0.804. This good agreement between the extinction retrievals for both instruments is a consequence of the very good agreement in default lidar ratio discussed in section 3.2.1.

## 5. Conclusion

[58] The Cloud Physics Lidar (CPL) provides "satellite-like" measurements but with higher SNR, higher resolution (both vertical and horizontal) and much lower multiple scattering than the CALIPSO lidar (CALIOP), making it arguably the most comprehensive validation tool for CALIOP cirrus cloud measurements and retrievals. The airborne CPL

was incorporated into a 2006 experiment (CC-VEX) specifically designed for this complex satellite validation. This paper focuses on the performance of three CALIPSO Level 2 products in comparison with like CPL products, specifically ice cloud lidar ratio, ice cloud extinction coefficient, and ice cloud optical depth. Ten coincident flight segments were analyzed, yielding over 13,000 in-cloud bins for each instrument and over 9,500 bins of collocated extinction coefficient where both instruments sampled in-cloud.

[59] Validating CALIOP extinction coefficients using CPL data is a complicated step beyond comparing the layer detection of the two instruments, which was performed by *Yorks et al.* [2011b]. The optical properties derived by the two instruments are not in agreement for horizontally oriented ice (HOI) as a result of the near-nadir viewing angle of CALIPSO during the CC-VEX project. Overall, HOI conditions result in a large decrease in average lidar ratio but not average extinction retrieved by CALIOP. This HOI issue has been removed in all CALIOP data sets obtained after the
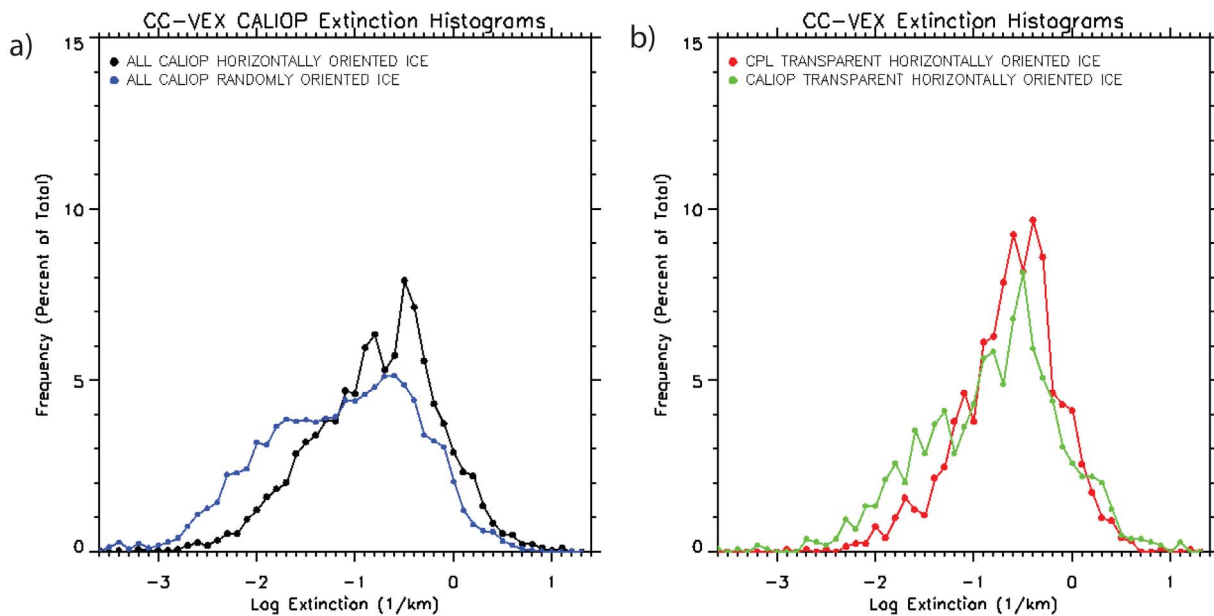


**Figure 12.** (a) The extinction distribution of CALIOP during HOI conditions (black) with the one from ROI conditions (blue). The HOI distribution results in more frequent high values compared to ROI conditions. The majority of HOI conditions encountered during CC-VEX are in opaque cloud layers, so the results would also trend higher for that reason. (b) CPL (red) and CALIOP (green) extinction distributions compare very well under transparent HOI conditions despite the fact that the average CALIOP lidar ratio is lower.

**Table 6.** Overall Average Optical Depths in Coincident Segments of CC-VEX

| Ice Cloud Category (Includes HOI and Opaque) | CPL Column Optical Depth (Above 8 km) | CALIOP Column Optical Depth (Above 8 km) | Average Optical Depth Relative Difference (%) |
|---|---|---|---|
| All Clouds | 0.703 | 0.688 | −2.185 |
| Night | 0.880 | 0.790 | −10.143 |
| Day | 0.584 | 0.618 | 5.969 |

change in laser tilt angle was implemented in November 2007. Furthermore, the CALIOP lidar ratio and extinction retrievals are significantly less than the CPL retrievals in opaque layers largely because the CALIOP data processing uses a different algorithm to retrieve optical properties in these opaque conditions, although the consequences of different penetration depths and the poorer SNR as complete attenuation of the signal is approached are also important. If the data is restricted to transparent randomly oriented ice (ROI) cloud cases using the proper CALIOP data flags, there is good agreement between instruments. Here, the mean
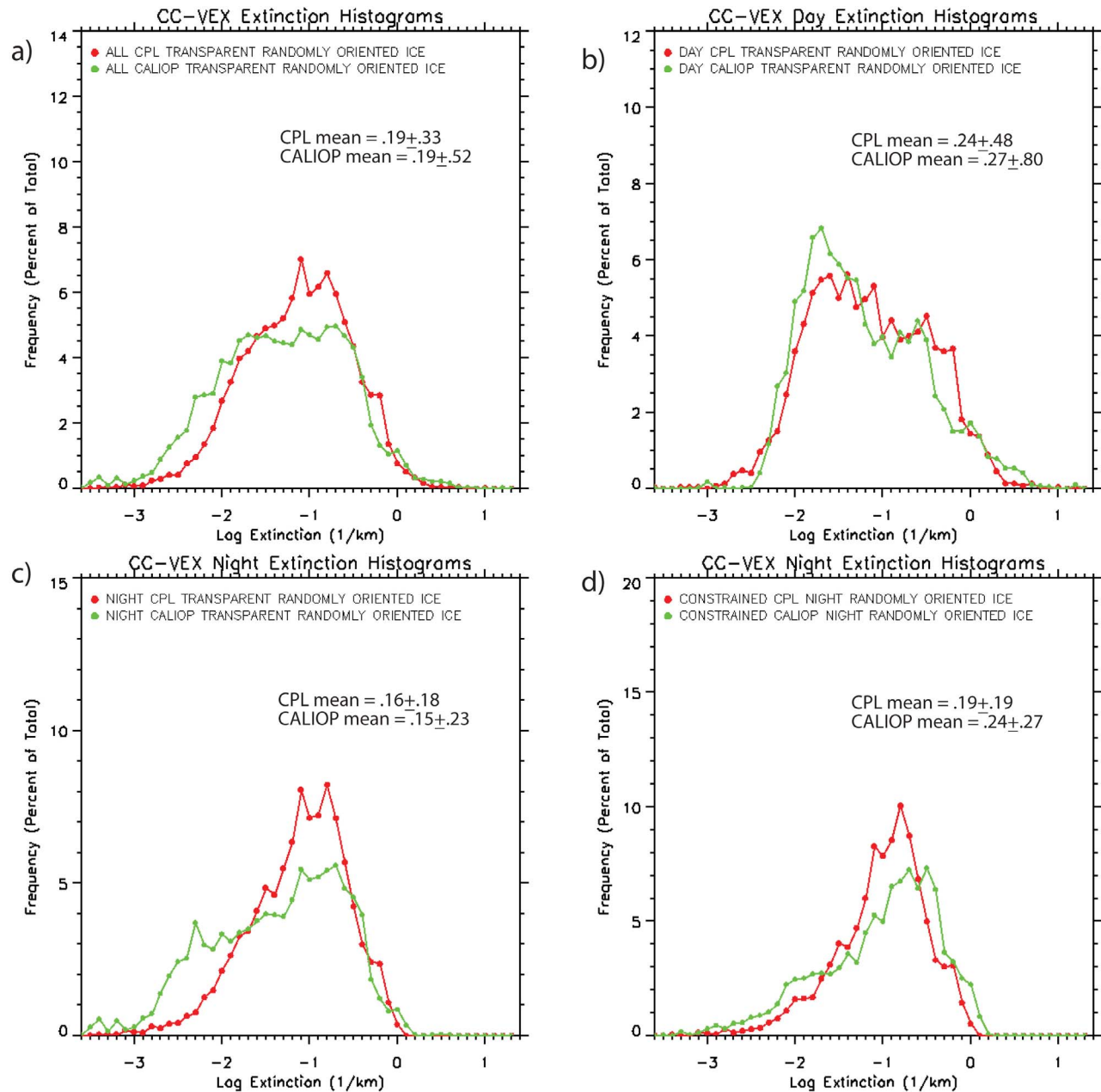


**Figure 13.** CPL (red) and CALIOP (green) extinction frequency distributions during CC-VEX coincident segments restricted to transparent ROI conditions only. (a) The overall distribution, (b) the daytime distribution, (c) the nighttime distribution, and (d) the distribution where only constrained lidar ratios are used.
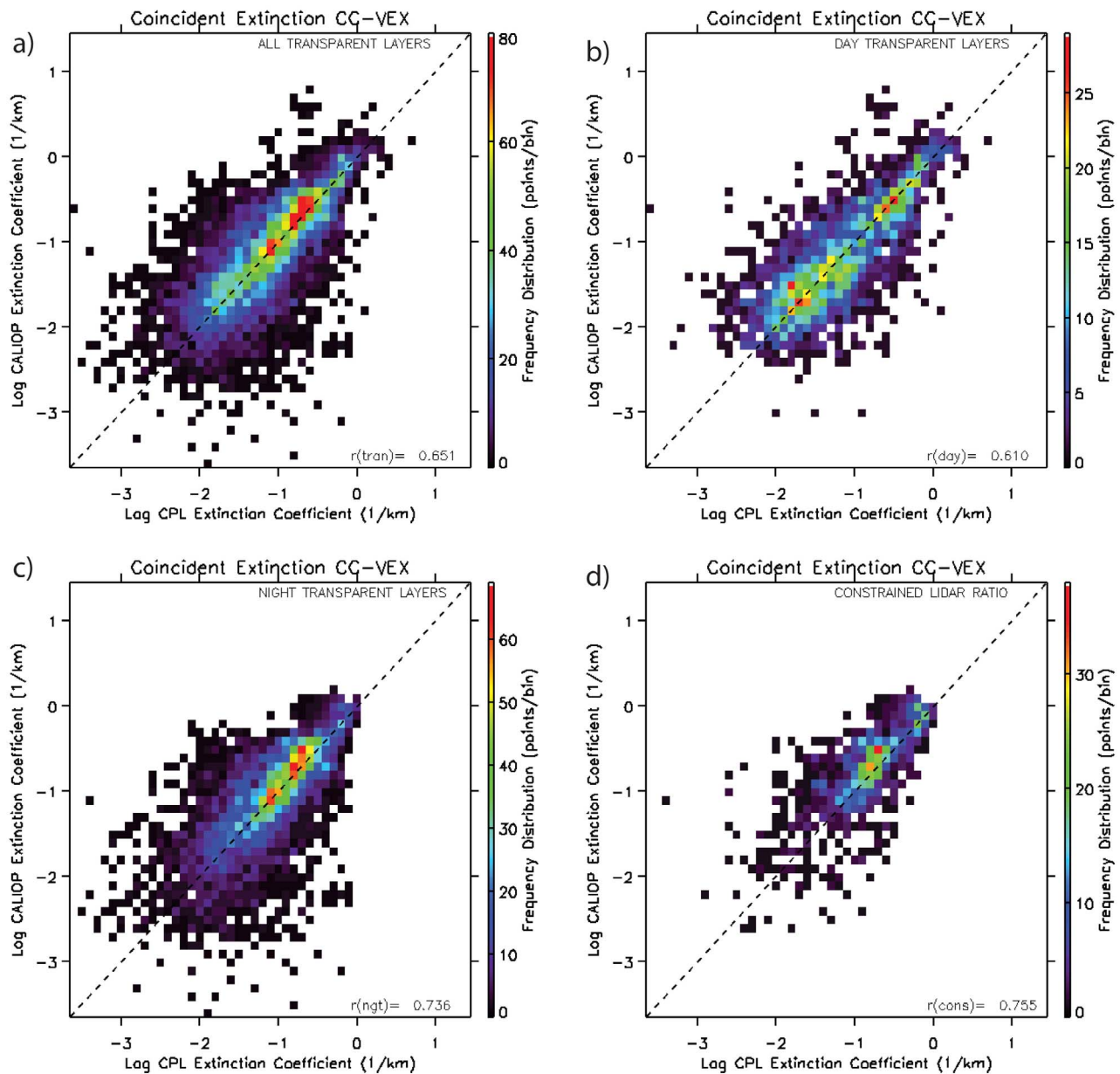
**Figure 14.** PDF distributions of extinction retrievals of coincident CC-VEX CALIOP-CPL point pairs restricted to transparent ROI conditions using colors to denote bin frequencies. (a) The overall distribution, (b) the daytime distribution, (c) the nighttime distribution, and (d) the distribution where only constrained lidar ratios are used.

CALIOP lidar ratio is within 2% of the CPL data set on average but is higher than CPL under certain constrained lidar ratio conditions. CALIOP transparent ROI extinction averages compare favorably overall to within 1% of CPL averages. When filtering the data further for exact coincident in-cloud point-pairs, the CALIOP retrieved extinction and optical depth average 15% above CPL values, partly due to higher average CALIOP attenuated backscatter used as inputs to the retrievals. There were diurnal differences in the transparent ROI coincident data as was expected, with best agreement at night when higher SNR causes less uncertainty in the attenuated backscatter. The generally good agreement between the two instruments found in this study for transparent ROI cloud conditions should give confidence to users of the CALIPSO data set to incorporate CALIPSO optical properties for transparent ROI cloud layers into their future studies.

[60] Results from this work show that when the lidar ratios of the two instruments are similar (within 1.5% such as with default lidar ratios), the resultant average optical depth difference is small (~7%) which leads to insignificant radiative flux discrepancies. However, when the lidar ratios do not agree (such as with the nighttime constrained cases where CALIOP is ~14% above CPL), the resulting optical depth difference is significant (31%), with 24% contributed to the lidar ratio difference. This difference leads to significant

radiative flux discrepancies (positive short wave and negative long wave). More research is needed to improve our understanding of the relationship between lidar ratio and cloud generation mechanisms, which consequently should improve the accuracy of cloud radiative forcing estimations from space-based lidars.

# References

Bissonette, L. R. (2005), Lidar and multiple scattering, in *LIDAR: Range-Resolved Optical Remote Sensing of the Atmosphere*, edited by C. Weitkamp, pp. 43–104, Springer, Berlin.

Das, S. K., C.-W. Chiang, and J.-B. Nee (2011), Influence of tropical easterly jet on upper tropical cirrus: An observational study from CALIPSO, Aura-MLS, and NCEP/NCAR data, *J. Geophys. Res.*, 116, D12204, doi:10.1029/2011JD015923.

Dupont, J.-C., M. Haeffelin, Y. Morille, V. Noel, P. Keckhut, D. Winker, J. Comstock, P. Chervet, and A. Roblin (2009), Macrophysical and optical properties of midlatitude cirrus clouds from 4 ground-based lidars and collocated CALIOP observations, *J. Geophys. Res.*, 115, D00H24, doi:10.1029/2009JD011943.

Eloranta, E. W. (1998), Practical model for the calculation of multiply scattered lidar returns, *Appl. Opt.*, 37, 2464–2472, doi:10.1364/AO.37.002464.

Elouragini, S. (1995), Useful algorithms to derive the optical properties of clouds from a backscatter lidar return, *J. Mod. Opt.*, 42, 1439–1446, doi:10.1080/09500349514551261.

Gayet, J.-F., G. Mioche, A. Dörnbrack, A. Ehrlich, A. Lampert, and M. Wendisch (2009), Microphysical and optical properties of Arctic mixed-phase clouds—The 9 April 2007 case study, *Atmos. Chem. Phys.*, 9, 6581–6595, doi:10.5194/acp-9-6581-2009.

Holz, R. E. (2002) Measurements of cirrus backscatter phase functions using a high spectral resolution lidar, M.S. thesis, Dep. of Atmos. and Oceanic Sci., Univ. of Wisconsin-Madison, Madison.

Hu, Y. (2007), Depolarization ratio–effective lidar ratio relation: Theoretical basis for space lidar cloud phase discrimination, *Geophys. Res. Lett.*, 34, L11812, doi:10.1029/2007GL029584.

Hu, Y., et al. (2007), The depolarization-attenuated backscatter relation: CALIPSO lidar measurements vs. theory, *Opt. Express*, 15, 5327–5332, doi:10.1364/OE.15.005327.

Hu, Y., et al. (2009), CALIPSO/CALIOP cloud phase discrimination algorithm, *J. Atmos. Oceanic Technol.*, 26, 2293–2309, doi:10.1175/2009JTECHA1280.1.

Hunt, W. H., et al. (2009), CALIPSO lidar description and performance assessment, *J. Atmos. Oceanic Technol.*, 26, 1214–1228, doi:10.1175/2009JTECHA1223.1.

Intergovernmental Panel on Climate Change (2007), *Climate Change 2007: The Physical Science Basis. Contribution of Working Group I to the Fourth Assessment Report of the Intergovernmental Panel on Climate Change (IPCC)*, edited by S. Solomon et al., Cambridge Univ. Press, Cambridge, U. K.

Jensen, E. J., L. Pfister, T.-P. Bui, P. Lawson, and D. Baumgardner (2010), Ice nucleation and cloud microphysical properties in tropical tropopause layer cirrus, *Atmos. Chem. Phys.*, 10, 1369–1384, doi:10.5194/acp-10-1369-2010.

Josset, D., J. Pelon, A. Garnier, Y.-X. Hu, M. Vaughan, P. Zhai, R. Kuehn, and P. Lucker (2012), Cirrus optical depth and lidar ratio retrieval from combined CALIPSO-CloudSat observations using ocean surface echo, *J. Geophys. Res.*, 117, D05207, doi:10.1029/2011JD016959.

King, M. D., et al. (1996), Airborne scanning spectrometer for remote sensing of cloud, aerosol, water vapor, and surface properties, *J. Atmos. Oceanic Technol.*, 13, 777–794, doi:10.1175/1520-0426(1996)013<0777:ASSFRS>2.0.CO;2.

Kuehn, R. E. (2001), A technique to measure cirrus cloud effective particle size using a high spectral resolution lidar, M.S. thesis, Dep. of Atmos. and Oceanic Sci., Univ. of Wisconsin-Madison, Madison.

Li, L., G. M. Heymsfield, P. E. Racette, L. Tian, and E. Zenker (2004), A 94 GHz cloud radar system on NASA High-altitude ER-2 aircraft, *J. Atmos. Oceanic Technol.*, 21, 1378–1388, doi:10.1175/1520-0426(2004)021<1378:AGCRSO>2.0.CO;2.

Marenco, F., V. Santacesaria, A. F. Bais, D. Balis, A. di Sarra, A. Papayannis, and C. Zerefas (1997), Optical properties of tropospheric aerosols determined by lidar and spectrophotometric measurements (Photochemical Activity and Solar Ultraviolet Radiation campaign), *Appl. Opt.*, 36, 6875–6886, doi:10.1364/AO.36.006875.

Martins, E., V. Noel, and H. Chepfer (2011), Properties of cirrus and subvisible cirrus from nighttime Cloud-Aerosol Lidar with Orthogonal Polarization (CALIOP), related to atmospheric dynamics and water vapor, *J. Geophys. Res.*, 116, D02208, doi:10.1029/2010JD014519.

McCubbin, I. B., et al. (2006), Overview of the multi-aircraft CALIPSO-CloudSAT Validation Experiment, *Eos Trans. AGU*, 87(42), Fall Meet. Suppl., Abstract A51E-0146.

McGill, M. J., D. L. Hlavka, W. D. Hart, V. S. Scott, J. D. Spinhirne, and B. Schmid (2002), The Cloud Physics Lidar: Instrument description and initial measurement results, *Appl. Opt.*, 41, 3725–3734, doi:10.1364/AO.41.003725.

McGill, M. J., D. L. Hlavka, W. D. Hart, E. J. Welton, and J. R. Campbell (2003), Airborne lidar measurements of aerosol optical properties during SAFARI-2000, *J. Geophys. Res.*, 108(D13), 8493, doi:10.1029/2002JD002370.

McGill, M. J., M. A. Vaughan, C. R. Trepte, W. D. Hart, D. L. Hlavka, D. M. Winker, and R. Kuehn (2007), Airborne validation of spatial properties measured by the CALIPSO lidar, *J. Geophys. Res.*, 112, D20201, doi:10.1029/2007JD008768.

Mioche, G., D. Josset, J.-F. Gayet, J. Pelon, A. Garnier, A. Minikin, and A. Schwarzenboeck (2010), Validation of the CALIPSO/CALIOP extinction coefficients from in situ observations in mid-latitude cirrus clouds during CIRCLE-2 experiment, *J. Geophys. Res.*, 115, D00H25, doi:10.1029/2009JD012376.

Nazaryan, H., M. P. McCormick, and W. P. Menzel (2008), Global characterization of cirrus clouds using CALIPSO data, *J. Geophys. Res.*, 113, D16211, doi:10.1029/2007JD009481.

Noel, V., and H. Chepfer (2010), A global view of horizontally oriented crystals in ice clouds from CALIPSO, *J. Geophys. Res.*, 115, D00H23, doi:10.1029/2009JD012365.

Piironen, P., and E. W. Eloranta (1994), Demonstration of a high-spectral-resolution lidar based on a iodine absorption filter, *Opt. Lett.*, 19(3), 234–236, doi:10.1364/OL.19.000234.

Platt, C. M. R. (1973), Lidar and radiometric observations of cirrus clouds, *J. Atmos. Sci.*, 30, 1191–1204, doi:10.1175/1520-0469(1973)030<1191:LAROOC>2.0.CO;2.

Platt, C. M. R. (1978), Lidar backscatter from horizontal ice crystal plates, *J. Appl. Meteorol.*, 17, 482–488, doi:10.1175/1520-0450(1978)017<0482:LBFHIC>2.0.CO;2.

Platt, C. M. R. (1979), Remote sounding of high clouds: I. Calculation of visible and infrared optical properties from lidar and radiometer measurements, *J. Appl. Meteorol.*, 18, 1130–1143, doi:10.1175/1520-0450(1979)018<1130:RSOHCI>2.0.CO;2.

Platt, C. M. R., N. L. Abshire, and G. T. McNice (1978), Some microphysical properties of an ice cloud from lidar observation of horizontally oriented crystals, *J. Appl. Meteorol.*, 17, 1220–1224, doi:10.1175/1520-0450(1978)017<1220:SMPOAI>2.0.CO;2.

Riihimaki, L. D., and S. A. McFarlane (2010), Frequency and morphology of tropical tropopause layer cirrus from CALIPSO observations: Are isolated cirrus different from those connected to deep convection?, *J. Geophys. Res.*, 115, D18201, doi:10.1029/2009JD013133.

Sassen, K., Z. Wang, and D. Liu (2008), Global distribution of cirrus clouds from CloudSat/Cloud-Aerosol Lidar and Infrared Pathfinder Satellite Observations (CALIPSO) measurements, *J. Geophys. Res.*, 113, D00A12, doi:10.1029/2008JD009972. [printed *114*(D8), 2009]

Schmid, B., et al. (2003), Coordinated airborne, spaceborne, and ground-based measurements of massive thick aerosol layers during the dry season in southern Africa, *J. Geophys. Res.*, 108(D13), 8496, doi:10.1029/2002JD002297.

Spinhirne, J. D., and W. D. Hart (1990), Cirrus structure and radiative parameters from airborne lidar and spectral radiometer observations: The 28 October 1986 FIRE study, *Mon. Weather Rev.*, 118, 2329–2343, doi:10.1175/1520-0493(1990)118<2329:CSARPF>2.0.CO;2.

Spinhirne, J. D., J. A. Reagan, and B. M. Herman (1980), Vertical distribution of aerosol extinction cross section and inference of aerosol imaginary Index in the troposphere by lidar technique, *J. Appl. Meteorol.*, 19, 426–438, doi:10.1175/1520-0450(1980)019<0426:VDOAEC>2.0.CO;2.

Spinhirne, J. D., W. D. Hart, and D. L. Hlavka (1996), Cirrus infrared parameters and shortwave reflectance relations from observations, *J. Atmos. Sci.*, 53, 1438–1458, doi:10.1175/1520-0469(1996)053<1438:CIPASR>2.0.CO;2.

Spinhirne, J. D., S. P. Palm, W. D. Hart, D. L. Hlavka, and E. J. Welton (2005), Cloud and aerosol measurements from GLAS: Overview and initial results, *Geophys. Res. Lett.*, 32, L22S03, doi:10.1029/2005GL023507.

Stephens, G. L., S. Tsay, P. W. Stackhouse Jr., and P. J. Flatau (1990), The relevance of the microphysical and radiative properties of cirrus clouds to

climate and climate feedback, *J. Atmos. Sci.*, 47, 1742–1754, doi:10.1175/1520-0469(1990)047<1742:TROTMA>2.0.CO;2.

Thorsen, T. J., Q. Fu, and J. Comstock (2011), Comparison of the CALIPSO satellite and ground-based observations of cirrus clouds at the ARM TWP sites, *J. Geophys. Res.*, 116, D21203, doi:10.1029/2011JD015970.

Vaughan, M., K. Powell, R. Kuehn, S. Young, D. Winker, C. Hostetler, W. Hunt, Z. Liu, M. McGill, and B. Getzewich (2009), Fully automated detection of cloud and aerosol layers in the CALIPSO lidar measurements, *J. Atmos. Oceanic Technol.*, 26, 2034–2050, doi:10.1175/2009JTECHA1228.1.

Wang, Z., and K. Sassen (2001), Cloud type and macrophysical property retrieval using multiple remote sensors, *J. Appl. Meteorol.*, 40, 1665–1682, doi:10.1175/1520-0450(2001)040<1665:CTAMPR>2.0.CO;2.

Winker, D. (2003), Accounting for multiple scattering in retrievals from space lidar, *Proc. SPIE Int. Soc. Opt. Eng.*, 5059, 128–139, doi:10.1117/12.512352.

Winker, D. M., W. H. Hunt, and M. J. McGill (2007), Initial performance assessment of CALIOP, *Geophys. Res. Lett.*, 34, L19803, doi:10.1029/2007GL030135.

Winker, D. M., M. A. Vaughan, A. Omar, Y. Hu, K. A. Powell, Z. Liu, W. H. Hunt, and S. A. Young (2009), Overview of the CALIPSO mission and CALIOP data processing algorithms, *J. Atmos. Oceanic Technol.*, 26, 2310–2323, doi:10.1175/2009JTECHA1281.1.

Winker, D. M., et al. (2010), The CALIPSO mission: A global 3D view of aerosols and clouds, *Bull. Am. Meteorol. Soc.*, 91, 1211–1229, doi:10.1175/2010BAMS3009.1.

Wu, D. L., J. H. Chae, A. Lambert, and F. F. Zhang (2011), Characteristics of CALIOP attenuated backscatter noise: Implication for cloud/aerosol detection, *Atmos. Chem. Phys.*, 11, 2641–2654, doi:10.5194/acp-11-2641-2011.

Yorks, J. E., M. McGill, D. Hlavka, and W. Hart (2011a), Statistics of cloud optical properties from airborne lidar measurements, *J. Atmos. Oceanic Technol.*, 28, 869–883, doi:10.1175/2011JTECHA1507.1.

Yorks, J. E., D. L. Hlavka, M. A. Vaughan, M. J. McGill, W. D. Hart, S. Rodier, and R. Kuehn (2011b), Airborne validation of cirrus cloud properties derived from CALIPSO lidar measurements: Spatial properties, *J. Geophys. Res.*, 116, D19207, doi:10.1029/2011JD015942.

Young, S. A. (1995), Analysis of lidar backscatter profiles in optically thin clouds, *Appl. Opt.*, 34, 7019–7031, doi:10.1364/AO.34.007019.

Young, S. A., and M. A. Vaughan (2009), The retrieval of profiles of particulate extinction from Cloud Aerosol Lidar Infrared Pathfinder Satellite Observations (CALIPSO) data: Algorithm description, *J. Atmos. Oceanic Technol.*, 26, 1105–1119, doi:10.1175/2008JTECHA1221.1.